SANDIA REPORT
SAND2012-1853
Unlimited Release
March 2012

Characterization of Failure Modes in Deep UV and Deep Green LEDs Utilizing Advanced Semiconductor Localization Techniques

Mary A. Miller, Edward I. Cole, Jr., and Paiboon Tangyunyong

Prepared by
Sandia National Laboratories
Albuquerque, New Mexico 87185 and Livermore, California 94550

Sandia National Laboratories is a multi-program laboratory managed and operated by Sandia Corporation, a wholly owned subsidiary of Lockheed Martin Corporation, for the U.S. Department of Energy's National Nuclear Security Administration under contract DE-AC04-94AL85000.

Issued by Sandia National Laboratories, operated for the United States Department of Energy by Sandia Corporation.

Available to DOE and DOE contractors from
U.S. Department of Energy
Office of Scientific and Technical Information
P.O. Box 62
Oak Ridge, TN 37831

Telephone: (865) 576-8401
Facsimile: (865) 576-5728
E-Mail: reports@adonis.osti.gov
Online ordering: http://www.osti.gov/bridge

Available to the public from
U.S. Department of Commerce
National Technical Information Service
5285 Port Royal Rd.
Springfield, VA 22161

Telephone: (800) 553-6847
Facsimile: (703) 605-6900
E-Mail: orders@ntis.fedworld.gov
Online order: http://www.ntis.gov/help/ordermethods.asp?loc=7-4-0#online

SAND2012-1853
Unlimited Release
March 2012

Characterization of Failure Modes in Deep UV and Deep Green LEDs Utilizing Advanced Semiconductor Localization Techniques

Mary A. Miller, Edward I. Cole, Jr., and Paiboon Tangyunyong
Validation and Failure Analysis, Org 1726
Sandia National Laboratories
P.O. Box 5800
Albuquerque, New Mexico 87185-MS1086

Abstract

We present the results of a two-year early career LDRD that focused on defect localization in deep green and deep ultraviolet (UV) light-emitting diodes (LEDs). We describe the laser-based techniques (TIVA/LIVA) used to localize the defects and interpret data acquired. We also describe a defect screening method based on a quick electrical measurement to determine whether defects should be present in the LEDs. We then describe the stress conditions that caused the devices to fail and how the TIVA/LIVA techniques were used to monitor the defect signals as the devices degraded and failed. We also describe the correlation between the initial defects and final degraded or failed state of the devices. Finally we show characterization results of the devices in the failed conditions and present preliminary theories as to why the devices failed for both the InGaN (green) and AlGaN (UV) LEDs.

ACKNOWLEDGMENTS

The authors are thankful for the assistance of Darlene Udoni for her technical support throughout this project, as well as Michael Rye and Paul Kotula for their expertise and materials characterization support. We also appreciate the backing of managers David Stein and Andy Boye throughout this work.

CONTENTS

1. Introduction 9
2. Technique and Methodology 11
3. Characterization at time zero 15
   3.1. Green Light-Emitting Diodes 15
   3.2. Ultraviolet Light-Emitting Diodes 21
4. Stress and Degradation of green and UV LEDs 29
   4.1. Green LEDs 29
      4.1.1. Stress conditions and changes over time 29
      4.1.2. Characterization of degraded green LED chips 31
   4.2 Degradation of UV LEDs 36
      4.2.1. Stress Conditions and Changes over time 36
      4.2.2. Failure in UV LEDs 38
      4.2.3. Characterization of failed UV LEDs 41
5. Summary, Conclusions, and Future Work 47
6. References 49
Distribution 50

FIGURES

Figure 1. Typical TIVA/LIVA imaging configuration incorporated into a scanning laser microscope 11
Figure 2. Scanning electron microscope (SEM) image of the n-type surface of a green LED showing the pyramidal structure roughness 15
Figure 3. Optical image of the n-type surface of a green LED (the bond pads and bond wires are located in the bottom right and left corners) 16
Figure 4. Typical IV curves and electroluminescence spectra from four different green LEDs measured at time zero 17
Figure 5. Light emission image of a green LED with 10 µA applied bias (bond pads appear dark and are located in the bottom left and right corners) 17
Figure 6. Reflected light image (left) and applied voltage map (right) of a typical green LED scanned with the 532 nm laser at 10 µA. Bright defect spots are indicated with white arrows. . 18
Figure 7. LE image taken at 10 µA bias of the same green LED shown in Figure 6. The dark spots indicate particles (purple arrows) on the surface. Only one of the bright spots in the AVM (Figure 6) show up in the LE image (indicated by the red arrow). All the other bright spots in the AVM are not observed in LE. 18
Figure 8. Reflected light image (left) and corresponding applied voltage map (right) of a shorted device scanned with the 532 nm laser 19
Figure 9. Applied voltage maps of a green LED at 100 µA (left) and 1 mA (right) indicating that some (red arrows) but not all defect sites change polarity with bias (blue arrows). 20
Figure 10. Typical IV curve and EL spectra for a 270 nm UV LED 21

Figure 11. Reflected light image (top left) and AVM (top right) biased at 10 µA and imaged with a 532 nm laser. Corresponding LE image (bottom) only shows one of the electrically active defects 22
Figure 12. Reflected light image (left) and corresponding applied voltage map (right) of an UV LED biased at 10 µA and imaged with a 532 nm laser 23
Figure 13. Control IV curves taken for five different UV LEDs indicating the position of the secondary slope 24
Figure 14. The relative intensity of a dark AVM site is plotted against the IV curve to show the correlation between defect signal strength and secondary slope 25
Figure 15. Left set of IV curves show the difference between a 532 nm laser spotted on the defect (solid line) and a control IV curve taken in the dark (dashed line). The right set of IV curves show the difference between a 532 nm laser spotted on the defect (dotted line), on the active area but far away from the defect (dashed line) and a control IV curve taken in the dark (solid line) for positive bias conditions. 26
Figure 16. AVMs indicating stress-induced changes of a green LED under 150 mA applied bias for 2 hrs 30
Figure 17. Reflected light image (left) and corresponding AVM (right) of a degraded green LED chip showing the large dark spots and haze. This AVM was taken with the 532 nm laser at 2 µA applied bias. 31
Figure 18. The left image is a cross-sectional SEM image of a stressed green LED showing a contact metallization defect. The right image shows TEM cross-sectional EDS mapping of different elements in the structure (Red = Sn, Blue = Pt-Sn-Ti, Green = W (Ti), Magenta = Pt-Sn, and Cyan = GaN) 32
Figure 19. AVM of an aged green LED characterized by cross-sectional TEM at the three indicated sites 34
Figure 20. TEM images of the dark defect spot (site 1) indicated in Figure 19 (right image shows the orange box at a higher magnification) 34
Figure 21. TEM cross-sectional images of site 2 (left) and site 3 (right) from Figure 19 35
Figure 22. UV LED aged at 30 mA for 20 hrs showing the reflected light image (left), AVM at 100 µA (middle), and at -0.6 µA (right) 37
Figure 23. UV LED aged at 50 mA showing the differences between time zero (middle image) and after 2 hrs of aging (right image). The AVMs were taken with the 532 nm laser with 10 µA applied bias. 37
Figure 24. Percent current increase produced by the 532 nm laser spotted on the AVM dark defect signal above that of the control IV curve for three aging conditions 38
Figure 25. Reflected light images and corresponding 532 nm AVMs (middle column: 0 µA applied bias, right column: 100 µA applied bias) of three different stressed parts (top: 50 mA-2 hrs, middle: 30 mA-100 hrs, bottom: -0.4 µA-25 hrs) 40
Figure 26. Aged UV LED at 50 mA for 15 hrs showing the one catastrophic failure site in both the reflected light image (left) and the AVMs (middle: no applied bias and right: 100 µA applied bias) with the 532 nm laser 41
Figure 27. Top: TEM Cross-sectional image of an UV LED aged at 30 mA for 5 hours cut through a dark defect signal in the AVM (the image is rotated so that the growth direction is from the right to the left of the image); Bottom: TEM cross-sectional image showing a high magnification view of the defect (normal orientation) 43
Figure 28. Cross-sectional TEM images of a failed UV LED aged at 50 mA for 5 hrs 45

TABLES

Table 1. Stress conditions of failed UV LEDs and the number of TIVA/LIVA defect signals at time zero..... 39

NOMENCLATURE

ADF	Annular dark field
AVM	Applied voltage map
EDS	Electron dispersive spectroscopy
EL	Electroluminescence
e-h	Electron-hole
FA	Failure Analysis
FIB	Focused ion beam
FWHM	Full width half max
IC	Integrated circuit
IV	Current-voltage curve
LE	Light emission
LED	Light-emitting diode
LIVA	Light-induced voltage alteration
PL	Photoluminescence
QW	Quantum well
SEM	Scanning electron microscope
SLM	Scanning laser microscope
TEM	Transmission electron microscope
TIVA	Thermally-induced voltage alteration
UV	Ultraviolet

1. INTRODUCTION

Group-III nitride light-emitting diodes (LEDs) have the potential to emit over the entire visible spectrum and well into ultraviolet (UV) wavelengths. The alloys of AlN, GaN, and InN possess tunable direct band gaps that can be tailored to specific wavelength energies with the correct choice of alloy compositions. Currently, the nitride-based LEDs are only commercially available between deep green (~540-550 nm) and deep UV (240 nm). In order to broaden the potential availability of these III-nitride LEDs, the reliability, lifetimes and low efficiencies in the deep UV and deep green LEDs must be addressed. These parameters are tightly coupled to key materials issues including the lack of native substrates, alloy separation during growth, the presence of non-radiative defects within the active region, inefficient p-type doping and hole-injection. The low growth temperatures required for higher indium compositions lead to poor crystalline quality and increased structural defect densities (V-defects) in green LEDs. At the same time, increased AlN compositions of AlGaN that are required for shorter wavelength devices are quite difficult to dope efficiently to reduce inherent resistance. Deep green and deep UV LEDs, which embody both ends of the current III-nitride LED commercially-available spectrum and exhibit the lowest efficiencies and poorest lifetimes, stand to gain the most from failure analysis (FA) studies. A driving force for efficient long-lifetime green LEDs is solid state lighting, while applications for deep UV are in water and air purification, bioagent sensing, and optical communications. This project utilizes existing non-destructive, laser-based techniques, such as thermally-induced voltage alteration (TIVA) and light-induced voltage alteration (LIVA), to detect and localize precursors to premature degradation and failure of deep green and deep UV LEDs.

Recent efforts to pinpoint specific causes for short lifetimes and poor reliability in deep green and deep UV LEDS have utilized such methods as time-resolved photoluminescence (PL), electroluminescence (EL), near-field scanning optical microscopy, cathodoluminescence and a variety of electrical measurements. Multiple degradation mechanisms have been proposed, including device self-heating,[1] an increase in non-radiative recombination,[2] compositional inhomogeneities,[3] Al atom migration from the *p*-cladding layer,[4] compensation of p-type doping or generation of point defects in the cladding layer,[5,6] and current crowding around contacts[7] as well as at macroscopic defects.[8] The degradation mechanism(s) occurring in the III-nitride devices are complex and may involve point-defects, making exact identification of those mechanisms quite difficult. Recent studies of UV LED degradation have identified a discrepancy between PL and EL measurements.[5,9,10] The degradation in PL (which targets the quantum wells) is either negligible or significantly less than the orders of magnitude decrease in photon counts encountered in the EL measurements. This suggests that the degradation is not occurring in the active region but more likely in the p-type cladding material increasing the number of nitrogen vacancies.[5,9,10] As defect signals are localized and observed by TIVA/LIVA in this work, these defect types and degradation mechanisms will be considered.

2. TECHNIQUE AND METHODOLOGY

In this work, the failure analysis (FA) techniques, TIVA and LIVA were applied to III-nitride light-emitting diode structures. LIVA and TIVA are scanning laser microscope (SLM) techniques where localized laser stimulation is applied to a device electrically biased in a constant current configuration in order to elicit an electrical response. Laser wavelengths can be either above (LIVA) or below (TIVA) the bandgap of the studied material. Interactions with the material generate electron-hole (e-h) pairs with LIVA or localized heating with TIVA. As the laser is scanned over the device, it interacts with the material highlighting areas with material defects. These interactions can be measured quantitatively by monitoring the voltage fluctuations on the constant current power supply which continuously changes as a result of the laser interactions. The voltage fluctuations in the device due to laser interaction are plotted spatially as a function of laser position, resulting in an applied voltage map (AVM) where a voltage change indicates the position of an electrically active site and perhaps a defect. TIVA and LIVA have already been established as effective tools in the localization of defects such as shorts or opens in Si-based integrated circuits, and in the identification of dislocation networks in vertical cavity surface emitting lasers.[11,12] Prior to this work, TIVA has only been used to image a catastrophic short demonstrated in a failed InGaN blue LED for the III-nitride material system.[13] Here, we utilize these failure analysis techniques on both deep green and deep UV LEDs to determine if defect signals can be observed, localized and identified in as-received commercial devices and can be labeled as precursors for premature failure in the devices. Figure 1 shows a schematic of a typical scanning laser microscope (SLM) setup configured for TIVA/LIVA imaging. The amplifier attached to the current supply is operated in the ac-coupled mode so that only variations in voltage, not the absolute voltage itself, are used to make the TIVA/LIVA images.

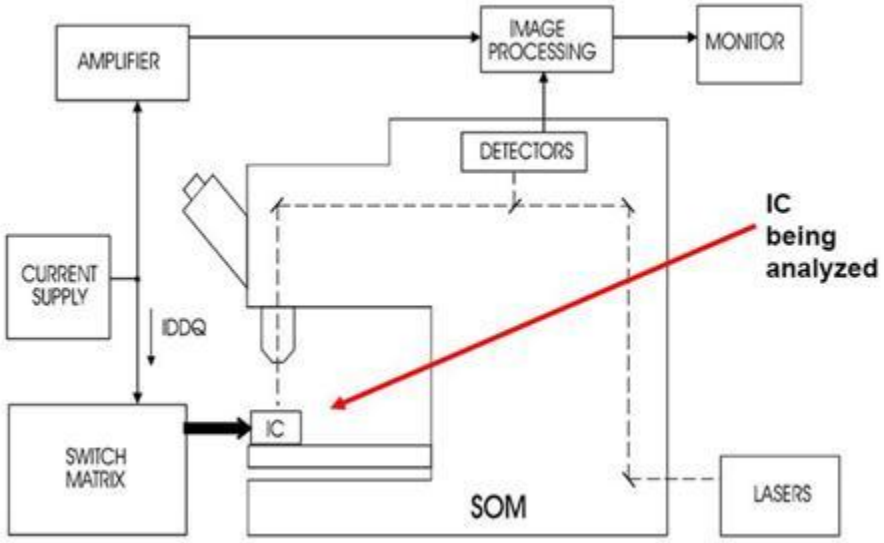

Figure 1. Typical TIVA/LIVA imaging configuration incorporated into a scanning laser microscope

An advantage of probing the devices with an optical source such as laser light is for these types of visible- and UV-wavelength devices, the active area and all of the individual InGaN or AlGaN layers can be probed with very little to no sample preparation. Most packaged LEDs are flip-chip devices; therefore, the lasers can probe the active regions of the device through the bottom of the substrate on which they were grown without having to penetrate through contact metallizations. For direct laser access all samples for this work were either packaged devices without lenses or devices in die form. Since LEDs are two terminal devices, electrical bias was easily applied to the parts.

The laser wavelengths in the scanning laser microscope available include 532 nm and 1064 nm (above bandgap for Si, LIVA), as well as 1340 nm (below bandgap for Si, TIVA). The LEDs analyzed in this work were commercial devices, with wavelengths near 525 nm and 270 nm. Only considering the ideal bandgap of the green and UV devices, all of the laser wavelengths would have less energy than the bandgap except for the green LED quantum well (QW). TIVA with localized heating would be the most likely laser interaction with the materials, providing a map dependent upon voltage fluctuations due to thermal heating of the device.

However, the devices are not ideal; threading dislocations, macroscopic defects, point defect mid-level states, and non-uniform metal/semiconductor contacts are all present. Other non-ideal properties include band bending near dislocation cores, carrier generation from mid-level states, increased current injection at metal/semiconductor interfaces with potential barriers below 2.3 eV and deep-level states that accommodate two-step electron-hole (e-h) pair generation between conduction and valence bands. These phenomena potentially can create energy levels within the bandgap of either the green or UV LEDs creating the potential for electron-hole pair generation and LIVA-like signals. With the longer wavelength laser energies, penetration all the way to the p-type contact is expected, so any of these defects/potential barriers may be encountered or activated with any of the lasers.

The presence of these potential defects, particularly threading dislocations, can present a very high background noise in LIVA/TIVA images and potentially mask signals from the electrically active defects that actually lead to premature failure (‘killer’ defects) or low efficiencies in the III-nitride devices. As will be shown in later sections, the presence of these background defects were not a problem in localization of the electrically active defects using LIVA/TIVA.

The parts analyzed were small enough that they could be scanned in one field of view. The Checkpoint SLM software provides real-time laser reflected-light images (optical images) as well as applied voltage maps (maps depicting voltage fluctuations due to laser interactions with the material and defects). This scanning method was the main mode of TIVA/LIVA imaging and characterization of the devices. Another technique to further characterize individual defect signals involved spotting the laser on one specific site. First, an applied voltage map (AVM) was acquired to localize electrically active defects within the device. Then the laser was positioned over the spot that showed either the dark or bright defect contrast. Instead of scanning, the laser stayed in the position over the defect signal while electrical measurements were taken. The idea was to further stimulate the defect observed in the AVM and provide quantitative evidence that

the defect changes the electrical characteristics of the device and thus can contribute to premature failure and/or poor reliability.

3. CHARACTERIZATION AT TIME ZERO

3.1. Green Light-Emitting Diodes

Purchased green LEDs were obtained in loose die or chip form—there was no packaging material to remove or deprocessing that occurred prior to analysis, but the chips had to be wire bonded in order to apply bias and electrical stress. The chips were n-side up; the n-type contact metallization was made up of two bond pads and lines that crossed the top surface of the chip. The surface was roughened, likely from laser lift-off and subsequent etching with a KOH-based treatment that gave the surface a pyramidal appearance (scanning electron microscope image in Figure 2). Roughening the surface of LEDs is a common practice to increase light output. However, any type of roughness on the surface of the chip will reduce the amount of laser light that penetrates the chip to the active area affecting both TIVA/LIVA sensitivity and resolution such that defect sizes may appear greater due to incident laser light refraction.

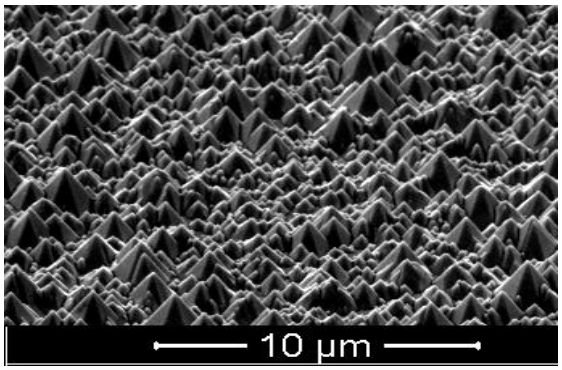

Figure 2. Scanning electron microscope (SEM) image of the n-type surface of a green LED showing the pyramidal structure roughness

The chips were bonded p-type GaN side down to Si for stability and the assembly then was bonded to a ceramic package where wire bonds were attached to the n-type contact pads. An optical image of a green LED chip (n-type GaN side up) is shown in Figure 3. The chip is roughly 1 mm on a side. The III-nitride composition makes up only about 10 µm of the entire chip thickness (~100 µm); the remaining thickness is made up of bonding metallization and Si substrate.

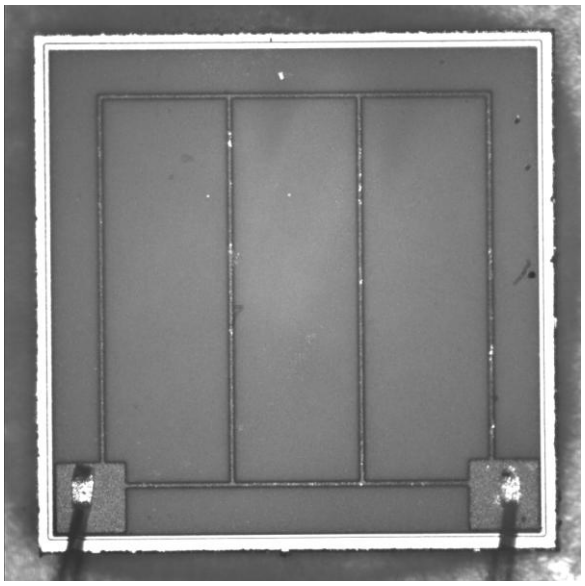

Figure 3. Optical image of the n-type surface of a green LED (the bond pads and bond wires are located in the bottom right and left corners)

Early electroluminescence spectra taken of the devices showed strong peaks near 520 to 525 nm, concurrent with the specification data provided with the purchased material. Current-voltage (IV) measurements were also taken of the devices prior to characterization or stressing. The IV measurements were swept from -3 V to 4.5 V. A typical spectra and IV curve are shown in Figure 4. The minimum current does not go through the zero-point on the x-axis. This could be due to the Si semiconductor bonded to the chip also undergoing biasing. The measurements were taken in the dark (un-illuminated device) and plotted on a semi-log plot to enhance the visualization of the subtle changes in the IV curves prior to turn-on of the device. After electrical characterization, the device was then characterized by light emission (LE). Light emission is a well-known failure analysis technique that detects photon emission from defects in silicon integrated circuits under bias using a very sensitive CCD camera. A typical LE image of a green LED is shown in Figure 5. The active area of the device is defined by the bright region. There is some spatial variation in the LE intensity with 10 μA of applied current. This was typical for all devices tested at low bias conditions, probably due to non-uniformities in the InGaN compositions or other inherent defects. Since no light penetrates through the metal bond pads, these appear dark in Figure 5. With 1 mA of applied current, the detector was saturated and these subtle, darker areas of the chip were no longer visible. Distinct dark features in the image were likely particles on the surface. Much like the bond pads they act like a mask through which the emission from the chip does not penetrate and therefore is not collected. The presence of these types of particles on the surface could be ascertained by their distinct edge (emission through the LED is somewhat diffuse due to the pyramidal surface structure) and lack of change with applied bias.

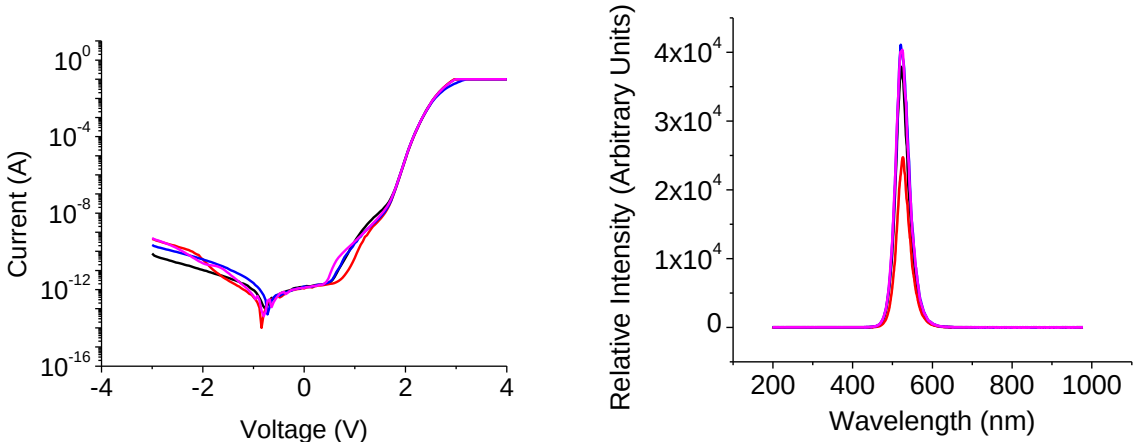

Figure 4. Typical IV curves and electroluminescence spectra from four different green LEDs measured at time zero

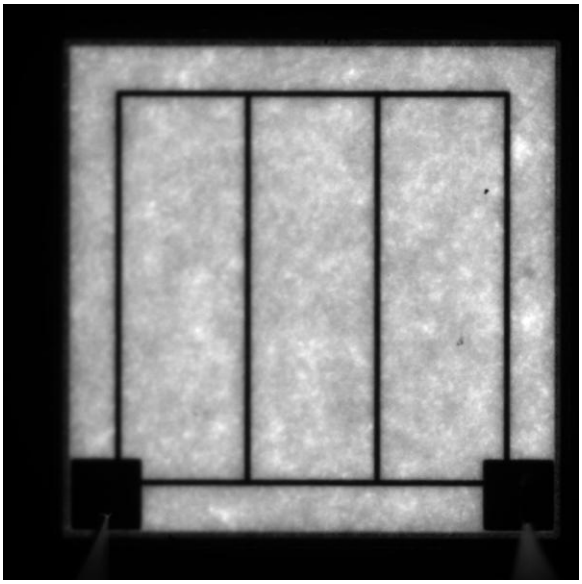

Figure 5. Light emission image of a green LED with 10 µA applied bias (bond pads appear dark and are located in the bottom left and right corners)

Electroluminescence, IV measurements and LE comprised the common characterization techniques applied to the devices at time zero. The next step was to apply TIVA and LIVA to determine if any new information could be obtained from the devices. Each chip was analyzed by TIVA/LIVA over a range of bias conditions from normal operating currents (350 mA) down to small reverse bias currents. Figure 6 shows the top-side reflected light and AVM of a green LED at 10 µA created with the 532 nm laser beam. The metal lines and bond pads appear black in the AVM. The small black spots are particles on the surface of the LED and are not electrically active defects (dark arrows in figure). The most interesting features of the AVM in Figure 6 are the small bright spots (white arrows). LE was used to characterize the same device

under a range of bias conditions to see if the same spots would be observed either by lack of light or by a bright signal (high current density, potentially a short). Of the six bright spots indicated in Figure 6, only one of them was indicated by dark contrast in the LE image (indicated by the red arrow in Figure 7). All of the other bright spots (orange arrows) were not detected in this manner. This was our first proof that the TIVA/LIVA technique may provide additional information in defect localization in III-nitride devices prior to failure.

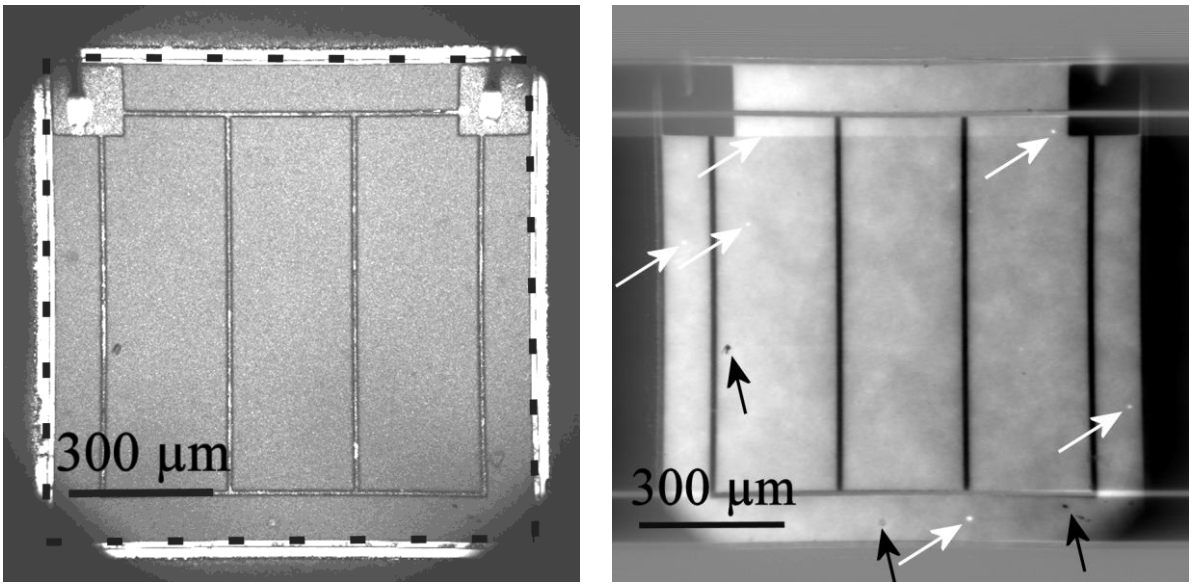

Figure 6. Reflected light image (left) and applied voltage map (right) of a typical green LED scanned with the 532 nm laser at 10 µA. Bright defect spots are indicated with white arrows.

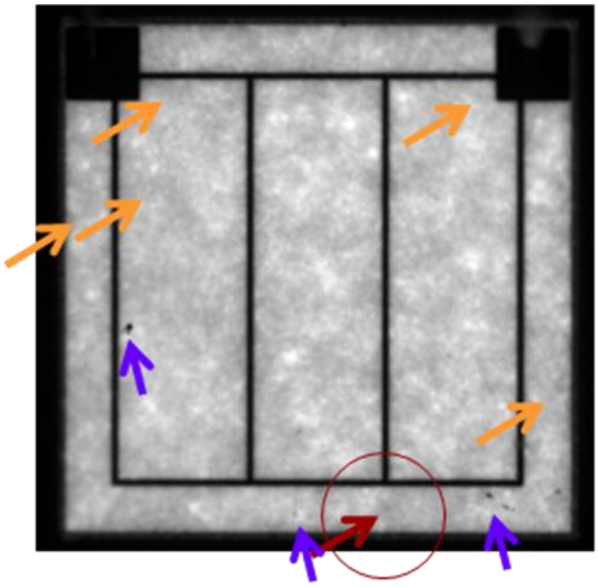

Figure 7. LE image taken at 10 µA bias of the same green LED shown in Figure 6. The dark spots indicate particles (purple arrows) on the surface. Only one of the bright spots in the AVM (Figure 6) show up in the LE image (indicated by the red arrow). All the other bright spots in the AVM are not observed in LE.

At the six bright spots in the Figure 6 AVM image, there were no corresponding physical defects that could be observed optically even at higher magnifications. Since the surface has been significantly roughened, it is possible that this roughness obscures the physical defect. The defect could also either reside within buried layers or may be too small for the resolution of the laser wavelength. Since the defect gave a bright signal in the AVM as the 532 nm laser was scanned across the device, the constant-current source momentarily drove the voltage up to compensate for a drop in power demand at the defect site. This suggests that at that site there is an increased resistance compared to the surrounding areas. When the same part was examined with the longer wavelength lasers, 1064 nm and 1340 nm, no defect signals (bright or dark) were observed. This was true even when significantly higher laser powers than those used for the 532nm AVMs were used (~10 mW at 1064 and 1340 nm compared to ~3 mW at 532 nm). This observation suggests a LIVA-photocurrent (versus TIVA-thermal) character to the bright spots. In terms of physical defects, bright spots in the AVM for InGaN-based LEDs could represent a number of different possibilities including threading dislocations, point defects, In segregation, or V-defects. If it is indeed a LIVA defect, this suggests a strong recombination site.

This type of bright defect spot, present in large numbers (10 to 40+ spots) and randomly dispersed across the device, was very typical for the green LEDs. A few chips, however, had a slightly different character when analyzed with the TIVA/LIVA technique. Some of the chips had no observable bright spots, but a very dark, intense signal (white arrow in Figure 8). The dark signals always accompanied an electrical signature (IV curve) that suggested a high current path existed through the LED. Figure 8 shows a cracked device with an intense dark signature in the AVM (indicated by the white arrow) which suggests a low resistance path compared to the surrounding material. The AVM signals from the rest of the chip are much weaker (can no longer make out the bondpads). Most of the charge is flowing through this path and the current density is lessened throughout the rest of the chip. This type of defect is highly visible under all three laser wavelengths due to the thermal signature that can be generated from it. However, the significance of the TIVA/LIVA scanning laser microscopy (SLM) technique is diminished for these types of parts, as this signal is easily obtained with LE and the electrical signal for a shorted device is obvious (high forward and reverse currents).

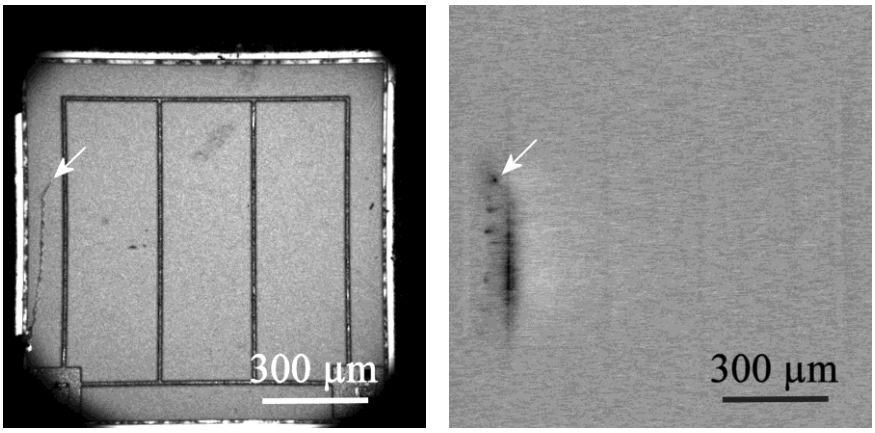

Figure 8. Reflected light image (left) and corresponding applied voltage map (right) of a shorted device scanned with the 532 nm laser

Typical bright defect spots as shown in Figure 6 were investigated more closely as a function of bias. Since they were only present under the 532 nm laser stimulation, the 1064 nm and 1340 nm lasers were not included in this part of the study. The range of bias conditions spanned from slight reverse biases to operating currents. For most chips it was determined that the bright signals remained at all ranges of bias conditions from reverse currents up until 1 to 5mA. It is theorized that at this point the background signal, due to the bias-induced band bending in the quantum wells, was enough to drown out the signal from the bright spots. It cannot be determined that the spots actually disappeared, only that the contrast from the defect signals was not enough to be seen independently from the background.

A few of the chips behaved in a slightly different manner. They still had multiple bright spots at low bias and slight reverse bias conditions and appeared independent of bias at low currents. However the bright spots changed polarities at higher currents (above 1 mA) and became dark defect sites. Typically this occurred for defect spots with the greatest intensity (greatest contrast in the AVM). In other words, those sites which were initially points of increased resistance at lower current became less resistive than the surrounding material and acted more like short paths at higher currents. At these higher current conditions some of these dark spots could be picked up with long integration times under the 1064 nm stimulation, suggesting more of a TIVA-thermal effect or leakage path. Figure 9 shows an example where some bright defects change polarity between 100 µA and 1 mA applied bias (red arrows). In addition, some of the spots that have bright contrast at 100 µA disappear at 1 mA (blue arrows). The results in Figure 9 suggest that there may be more than one defect type that creates a bright contrast, or that there are some defects that are more extensive (more degraded) than others and only these can be seen to switch polarity.

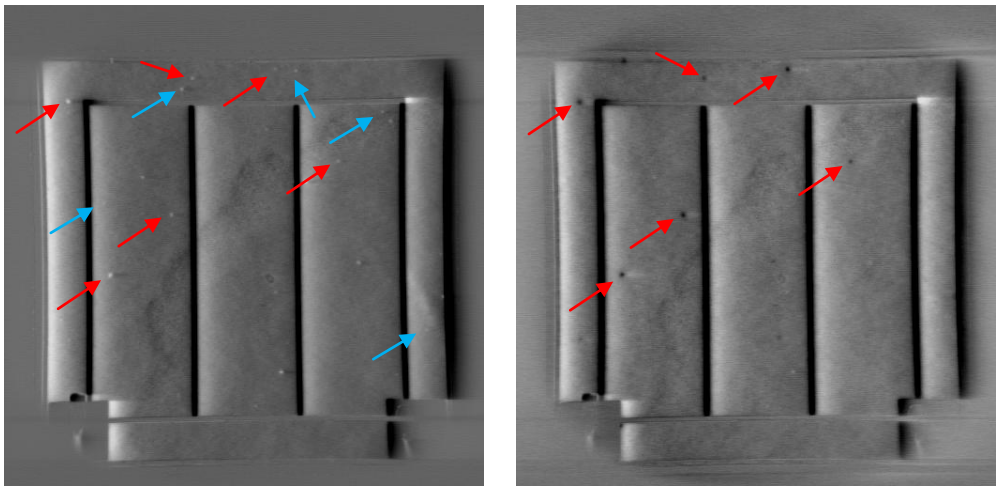

Figure 9. Applied voltage maps of a green LED at 100 µA (left) and 1 mA (right) indicating that some (red arrows) but not all defect sites change polarity with bias (blue arrows).

The characterization of the bright defect spots, the shorted dark defect spots and those that changed polarity with bias were all recorded as initial green LED behavior. It was important to monitor the changes in defect spots under stress as a function of current and laser wavelength. Those devices that were already shorted were removed from the study. The bright defect spots

could potentially be precursors to early failure in the green LEDs. The potential defects and degradation mechanisms are discussed in a later section.

3.2. Ultraviolet Light-Emitting Diodes

Like the green LEDs, the UV LEDs were characterized at time zero to determine if the TIVA/LIVA technique would be able to identify electrically active defects within the wide bandgap material. Analysis of this material was even more difficult since the bandgap energy was significantly higher than the energies available with the three lasers and band-bending that may have produced LIVA signals in the green LEDs was not likely to produce LIVA signals in the UV LEDs.

Commercial UV LEDs were purchased prepackaged in TO-39 cans, with the can and lens removed for ease of access and characterization. They were flip-chipped with polished backsides, so optical inspection all the way through the device to the p-type contact was straightforward. All of the TIVA/LIVA work was also done through the backside of the chip, as will be indicated in the next few figures. First, the electroluminescence spectra and IV measurements were taken of the devices at time zero and one example is shown in Figure 10. The IV curves were plotted on a semi-log plot to accentuate the subtle differences at low voltages prior to device turn-on. The EL spectrum shows a strong signal near 270 nm for this particular part. In the inset of the spectra there is a small shoulder in the UV LED spectra, slightly blue-shifted.

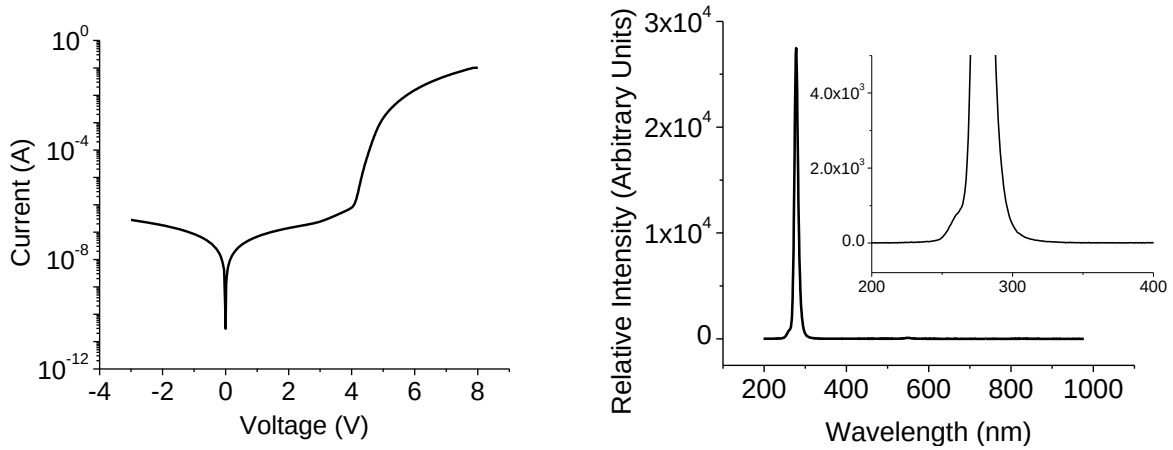

Figure 10. Typical IV curve and EL spectra for a 270 nm UV LED

Figure 11 shows a reflected light image and AVM of an UV LED imaged with the 532 nm laser. The definitive features in the images are the active region (dumbbell-shaped mesa) and the contrast between n-type (outer) and p-type (inner) contacts. Ideally, the epilayers would all be transparent to the 532, 1064, and 1340 nm lasers. However, the 532 nm laser has articulated two electrically active sites within the device (Figure 11, top right image), shown as dark spots. If the defects were thermally stimulated (TIVA), then the spots could represent leakage paths with a much lower resistance than the surrounding regions, and the longer-wavelength lasers should

also stimulate dark signals. Some of the UV LEDs, however, showed dark signals only with the 532 nm laser. No signals with the 1064 nm and 1340 nm lasers were observed even when higher laser powers were used (up to 10mW compared to 3mW for the 532nm laser). This suggests that there might be an electron-hole (e-h) pair generation component to the signals. In other devices, the dark signals were visible with all three lasers (532, 1064 and 1340 nm) but the intensity of the dark spot was much stronger with the 532 nm laser. A possible scenario might entail a two-step e-h pair generation process involving a deep level defect that is very near the middle of the bandgap or a metal/semiconductor junction with activation energy greater than that of the 1064 nm laser.

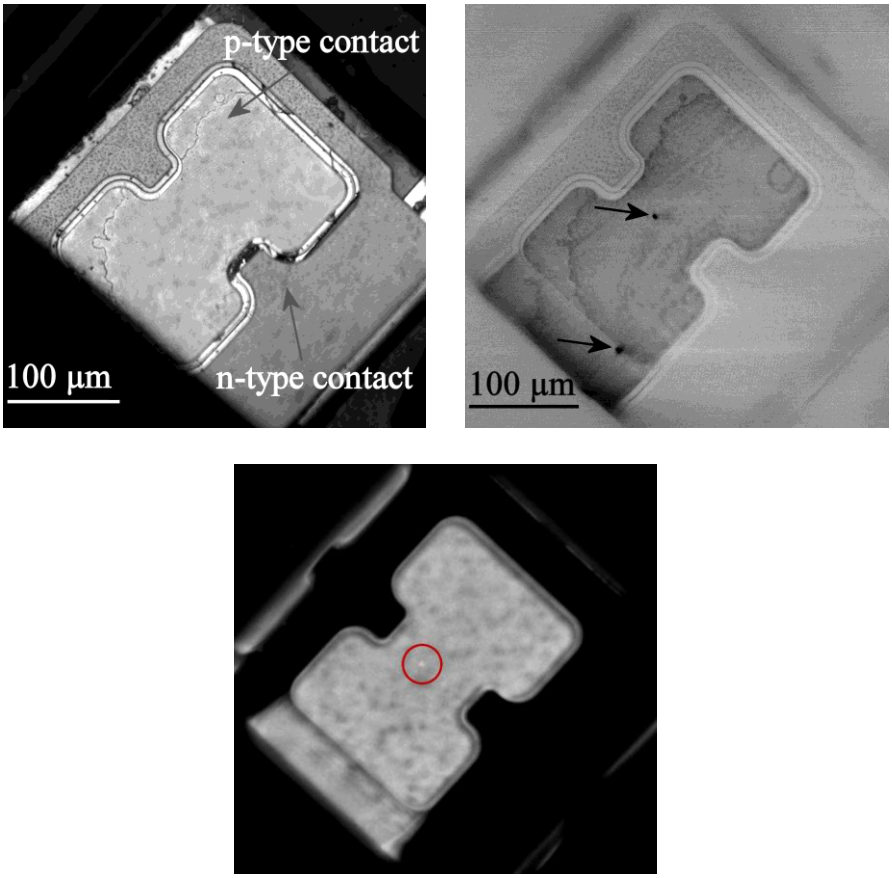

Figure 11. Reflected light image (top left) and AVM (top right) biased at 10 µA and imaged with a 532 nm laser. Corresponding LE image (bottom) only shows one of the electrically active defects

The bottom image shown in Figure 11 is an LE image of the same device. There is an obvious bright spot indicating the presence of one of the two TIVA/LIVA defects. The spot is bright in the LE image suggesting a high current density. The actual wavelength of the emitting defect light is unknown and the intensity of the defect was such that it could not be identified from the QW emission by EL. This bright spot in the LE image (indicated by the open red circle) corresponds to a dark defect signal in the AVM in Figure 11. However, regardless of the bias input to the device, the other defect spot easily shown in the AVM does not appear in the LE

image. Once again this proves the usefulness of the TIVA/LIVA method in defect localization in the III-nitride materials.

On closer examination of the reflected light image at higher magnifications, there was physical evidence of a defect site which matched the positions of the dark signals in the AVM (Figure 12). What is interesting about this set of images is that there are a large number of optically similar sites in the same field of view and the TIVA/LIVA technique was able to pinpoint the one electrically active site.

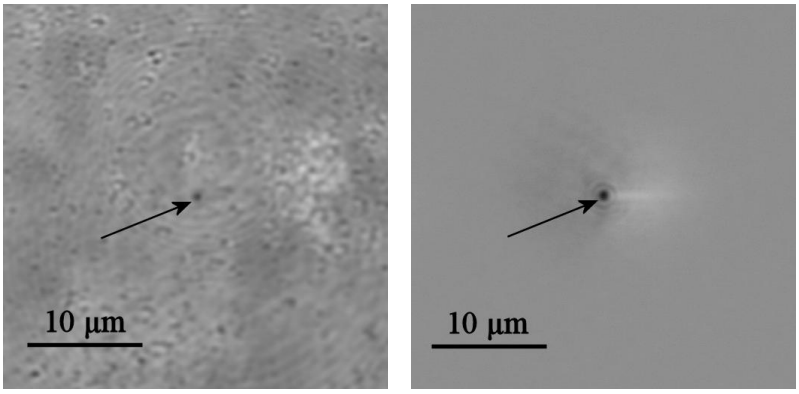

Figure 12. Reflected light image (left) and corresponding applied voltage map (right) of an UV LED biased at 10 µA and imaged with a 532 nm laser

Of the 15 LEDs tested in this work, all but two devices indicated 1-4 dark defect spots under 532 nm laser stimulation. Unlike the green LEDs, the defect signal strength was dependent upon the applied bias to the device. At zero applied bias or under reverse bias conditions defect spots were not visible in the AVM under stimulation from any of the three laser wavelengths. Defects were only visible under slight positive bias conditions. Under the 532 nm laser, the defects consistently became visible with a turn-on bias of about 0.4 to 0.6 µA (~3 V), regardless of spatial position (mesa edge or active region). The signal strength of the defect (contrast in the AVM) then increased steadily above the turn-on bias and appeared to peak near 1-2 µA (~4 V) and then dropped off with increasing bias. In some devices, the defect spot would disappear into the background signal intensity near 1-5 mA of applied bias, while other defects remained faintly visible up to operating currents (20 mA).

When this data was coupled with the time-zero IV curves, a very interesting correlation was revealed. Current-voltage sweeps (or IV curves) were measured for all of the UV LED devices prior to any stress or aging. The sweeps covered a voltage range from -3 V up to 8 V. The curves were very similar from device to device except for the voltage range between about 3 and 4 V. In this range an abrupt change in slope (plotted with the log of current) is observed just prior to the device turn-on voltage. This slope change was observed in several devices as shown in Figure 13. This part of the IV curve between 3 and 4 V is referred to as the secondary slope. On closer examination, it was determined that the start of the secondary slope coincided with the defect turn-on bias in the 532 nm AVM. For purposes of further comparing the signal strength to the IV curve, the signal intensity of the defect was normalized to the peak intensity and plotted as a function of voltage on the same voltage axis as the IV curve. The plot in Figure 14 shows a

strong correlation between defect intensity and secondary slope in the IV curve. As suggested, the onset of the secondary slope in the IV curve matched up with the observance of the dark defect spot. The peak intensity also coincided with the termination of the secondary slope or the device turn-on voltage. It is suggested that this increased current or secondary slope in this portion of the IV curve is then directly related to the presence or absence of electrically active sites observed in the AVM.

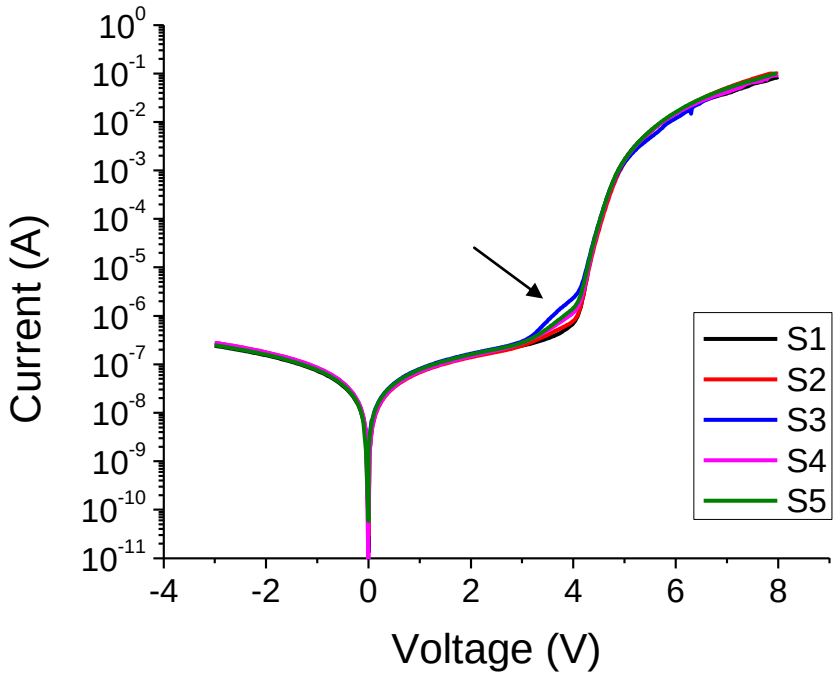

Figure 13. Control IV curves taken for five different UV LEDs indicating the position of the secondary slope

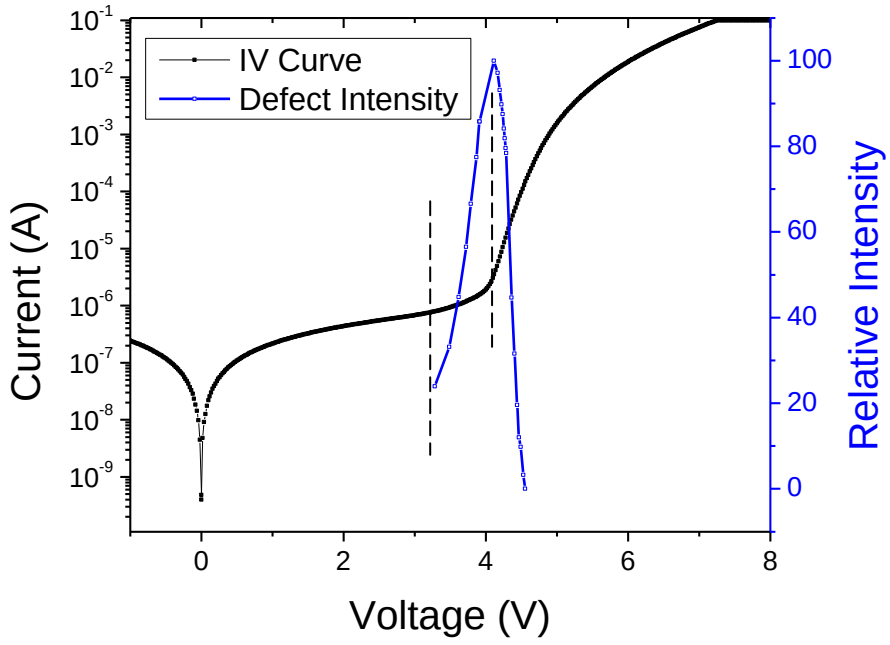

Figure 14. The relative intensity of a dark AVM site is plotted against the IV curve to show the correlation between defect signal strength and secondary slope

All UV LEDs with dark defect spots in their AVMs had IV curves with a secondary slope located between 3 and 4 V. The slope of the curve in this voltage range (secondary slope) was generally steeper for devices with a greater number of defects. Also, the slope was steeper for devices with more active area defects compared to devices with the same number or fewer mesa edge defects. The more dark defects that were present, the higher the leakage current in the device. Those devices that did not show a secondary slope in their IV curves did not have defect signals in their AVM. If the defect signal originated from deep level defects that allowed a two-step e-h pair generation condition, the leakage would be more constant and less bias-dependent (or diode-like in behavior). This type of behavior suggests more of an activation event such as current injection into a metal/semiconductor potential barrier.

One last method of characterizing the devices using the TIVA/LIVA technique involved spotting the laser directly on the contrast site while the IV curve was measured. In this way, a measure of how effective the laser wavelength was in stimulating the defect by comparison to the surrounding material and control IV curve was obtained. The left graph in Figure 15 shows the difference between a device IV curve taken in complete darkness compared to an IV curve taken when the laser is spotted directly on the TIVA/LIVA signal spot. There appears to be a nonuniform increase in current, primarily confined to the range between -3 and 4 V. Interestingly, the secondary slope increased when spotted with the laser, suggesting a localized increase in current due to stimulation of the contrast site. To separate the effects of laser stimulation of the defect itself compared to the surrounding 'defect-free' material, the laser was also spotted off of the contrast site (referred to as "off of defect" in the figure), more than 100 µm away while the IV curve was measured. The right image in Figure 15 shows all three

conditions in a smaller positive voltage range from 0 to 6 V. When the laser was spotted on the active area but away from the defect, the same increase in current is apparent up until near 3 V (onset of secondary slope). At reverse bias conditions, the increase in current is also visible but there is no difference between laser spotting on the defect and off of the defect (not shown). This suggests that there is an overall increase in leakage current of the device under stimulation with the 532 nm laser. This type of behavior could be due to deep level states since the effect is the same regardless of laser spotting position. It was initially thought that this increase in current was due to increased current injection at the p-type GaN/metallization interface, however spotting the laser outside the active region elicits the same response. This result suggests that it is not current injection at the metal/semiconductor interface but something inherent in the material itself producing the elevated current. It is also not likely that this increase in current is related to leakage at the mesa edge since the active-area defect is the one that is probed, far away from the mesa edge and diffusion lengths in AlGaN materials are relatively small (orders of magnitude less than the distance to the mesa edge). This is in disagreement with literature with results that describe increased tunneling currents prior to device turn-on are due to surface leakage at the mesa sidewalls.[9] Within the secondary slope voltage range, the laser has little to no effect on the slope if spotted far away from the defect, but a significant effect if spotted directly on the defect.

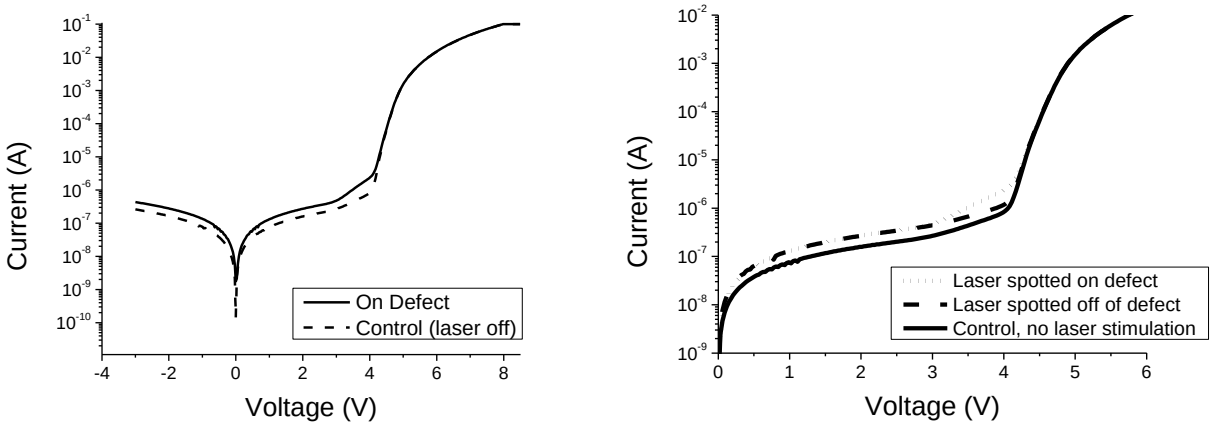

Figure 15. Left set of IV curves show the difference between a 532 nm laser spotted on the defect (solid line) and a control IV curve taken in the dark (dashed line). The right set of IV curves show the difference between a 532 nm laser spotted on the defect (dotted line), on the active area but far away from the defect (dashed line) and a control IV curve taken in the dark (solid line) for positive bias conditions.

The effect of laser spotting on the secondary slope was most pronounced with the 532 nm laser and much less with longer-wavelength lasers. This wavelength dependency suggests some potential barrier or deep level states with activation energies greater than that supplied by the 1064 nm laser are present for the dark defect spots in the UV LEDs. To monitor the device degradation throughout aging, IV curves with and without laser spotting were acquired.

The target devices were stressed at nominal and accelerated current densities to decrease time to failure. The bias conditions included 30 mA, 50 mA and 70 mA. Stress time continued until device failure indicated by electrical shorts or significant loss of EL (>50%).

4. STRESS AND DEGRADATION OF GREEN AND UV LEDS

4.1. Green LEDs

4.1.1. Stress conditions and changes over time

Over 30 green LEDs were analyzed in this work. The devices had been purchased in die form and bonded into a ceramic package. Since the devices had not been packaged with a heat sink, aging near operating currents of 350 mA immediately evidenced signs of extreme thermal damage. To reduce the thermal damage, bias conditions as low as 150 mA were used to age or stress the parts. Devices were also air-cooled during stress to reduce thermal damage. Parts were aged for up to 200 hrs or until failure occurred. Throughout aging, the IV curves, TIVA/LIVA scans and intermittent EL spectra were monitored for changes that would indicate premature failure. Since these devices were not prepackaged, thermal degradation was believed to have a significant contribution.

Several interesting results were observed in the green LED AVMs during aging. In some of the parts there were no changes in the AVM images; for example, initial bright defect spots remained bright during aging and there was no significant change in the contrast of these defects. In addition, no new spots were observed in these samples and changes in other measured parameters were minimal. Slight increases in current over time, typically at voltages smaller than the turn-on voltage of the device, were observed. This increase in current could only be measured in the dark with long integration times; the base current was on the order of 10^{-13} to 10^{-12}A.

In other devices, catastrophic shorts occurred under stress. The shorts were easily observed in the AVM images using the 532 nm and longer-wavelength lasers. In addition, a drop in measured voltage at a given current bias and a drop in EL intensity were observed. Typically LE images taken of these devices showed bright defect spots which matched the position of dark defect spots in the AVM.

Yet other chips developed marbled or hazy AVM images, evolving spatially from underneath the bondpads and spreading outwards. This type of stress caused IV curves to exhibit a slight increase in leakage current at voltages below turn-on as well as decreased current at higher voltages. Those bright spots that were originally located in the haze area disappeared after stress; sometimes new spots appeared within the haze. The haze region was dark in the LE image sometimes with a boundary punctuated by multiple bright spots.

Another stress-induced change observed in the green LEDs involved the appearance of large macroscopic darkened spots that could be seen both in the AVM and in the reflected light image. They were typically circular or extended out from the edges of the bondpads. Since the large, dark spots could be seen optically, they might be related to changes in the p-type contact metallization beneath the chip. There was an increase in the overall size and sometimes number of these macroscopic spots with aging.

Finally, some chips exhibited an increased number of defect sites with aging. Some of them were dark, some bright. The bright spots tended to have a dark halo appear around the bright center at higher applied biases. In this work, the most interesting cases were the observance of new signals, whether they were the large dark spots, hazed regions, or new bright spots with dark halos. In Figure 16 the difference between a chip at time zero and the same chip after aging at 150 mA for 2 hrs is shown. In this case, haze (indicated in the area above the orange dashed line), new bright defect spots (pink arrows), and a new bright defect spot with a dark halo have developed. The blue arrows indicate the original bright defect spots and also indicate those that did not change in the second aged image. Both of the AVMs were taken at 100 µA scanned with the 532 nm laser (~3 mW). In Figure 17, the larger dark spots can be seen in both the reflected light image as well as the AVM. These images were taken with the 532 nm laser under 2 µA applied bias. Within the hazed area the defect signals appear brighter, indicating a higher resistance path than the surrounding material. This particular device was aged 100 hrs at 3.4 V (250 mA).

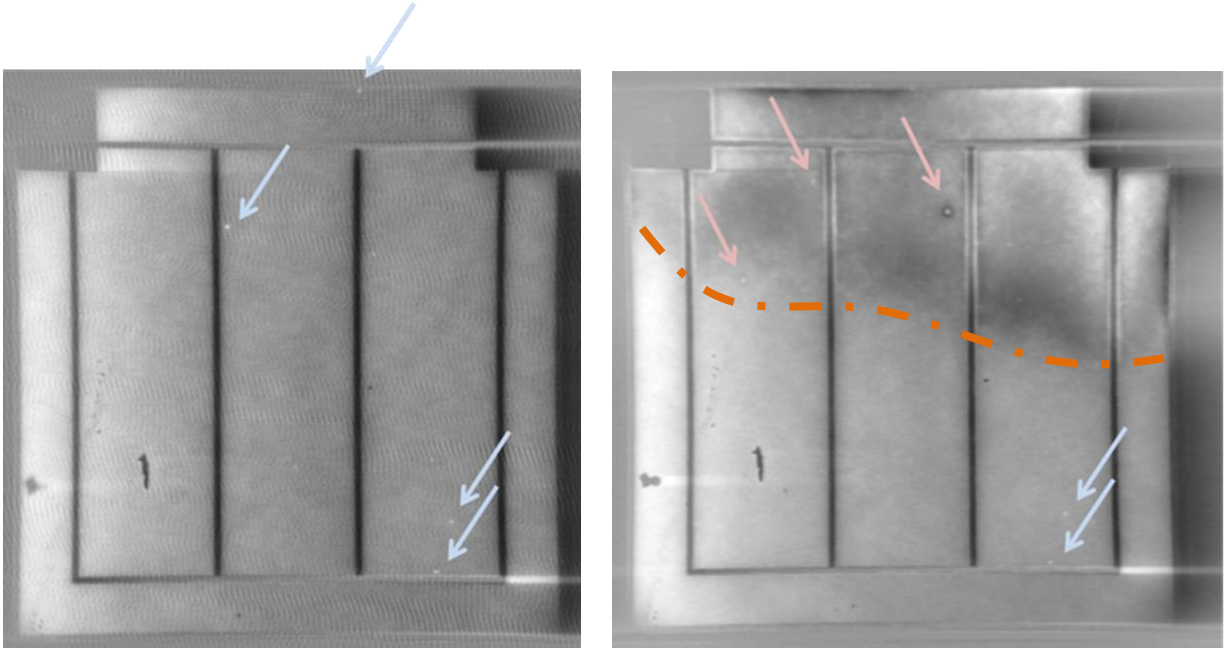

Figure 16. AVMs indicating stress-induced changes of a green LED under 150 mA applied bias for 2 hrs

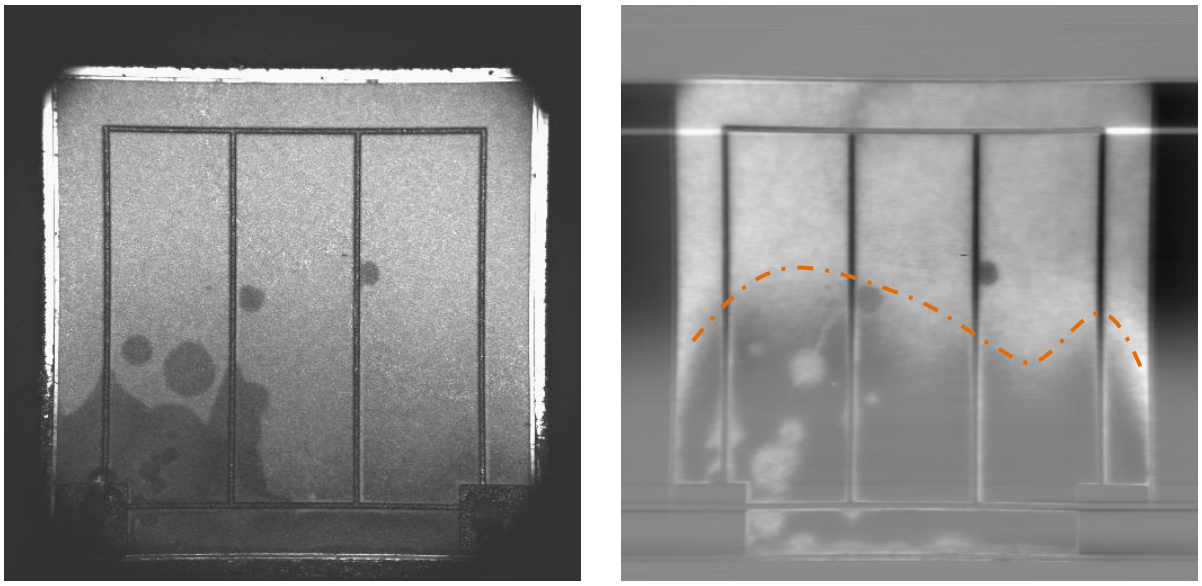

Figure 17. Reflected light image (left) and corresponding AVM (right) of a degraded green LED chip showing the large dark spots and haze. This AVM was taken with the 532 nm laser at 2 µA applied bias.

4.1.2. Characterization of degraded green LED chips

In order to understand the signals that were generated in the AVMs, focused ion beam (FIB) removal and thinning of the area of interest was required for detailed structural analysis of the defects either in the scanning electron microscope (SEM) or the transmission electron microscope (TEM). FIB cross-sections were removed from most of the defect areas for materials characterization.

The first site discussed is the larger, circular dark spots as shown in Figure 17. The SEM cross-sectional image in Figure 18 shows the green LED cross-section, the contact metallization and bonding metal to the Si chip below. Characteristic V-defects begin in the n-GaN and proceed through the InGaN/GaN quantum wells into the p-GaN. This image cannot resolve the individual QW layers but this is not the focus of the image. Since this is a flipped device, the growth occurs from the top of the image (n-GaN) to the bottom of the image (p-GaN and subsequent metallization). Deposition of the multilayer metallization occurred prior to the bonding of the chip to the Si substrate. The light-colored layer of metal in Figure 18, which comprises the composition of the inner sphere of multilayer metallization, was deposited first, followed by the discrete layers that coat the sphere as the metallization is deposited or developed. This contact metallization sphere matches the center of the large dark defect spots seen in the AVM (Figure 17). Since the defect spots are dark in the AVM, it suggests a decreased resistance path for charge flow. It is suggested that with aging the layers intermix and react (note the Kirkendall voids at the end of the reaction regions in the individual metal layers) which change the metallization at the metal/semiconductor interface. If the new metallization has a lower potential barrier, the current density will be greater at that junction then at the surrounding interface. Due to the growth geometry of the metal layers, it is unlikely that this spherical aberration occurred during stress of the device and likely evolved from a metal droplet (most

likely Pt) left on the surface of the first layer of metal. However, the reaction of the metal layers, through diffusion at the pinched edges of the multiple layers as they surround the sphere, caused a change in the metallization such that over time, the TIVA/LIVA technique identified the anomaly. The initial metallization structure, starting at the semiconductor interface and proceeding downwards in the image is as follows: Ag-Au/W/Pt/W/Pt/W/Pt/W/Pt/W/Pt-Ti/Sn. The Sn diffused and reacted with the Pt and Ti creating the thickened lighter contrast layers. The initial thickness of the Pt layers can be seen at the left and right edges of the image (very bright contrast). Also in Figure 18, an EDS image is shown from the TEM cross-section of the defect. The reacted layers appear to be Pt and Sn with minor amounts of Ag (shown in magenta), while the W layers remain largely intact (green in the image). The center of the defect appears to be entirely reacted Pt and Sn. Initially the multiple Pt/W layers were probably diffusion barrier layers used to reduce reaction of a common bonding metal (Sn) with the contact metallization. However due to the presence of the metal droplet and pinching of the layers around the droplet, the diffusion barrier layers could not provide adequate protection from Sn diffusion. TEM images of the InGaN/GaN QW region directly above the metallization defect did not show anything significantly different than regions that were far away (not shown). Therefore it is suggested that the dark defect spots appeared due to changes in the p-type semiconductor/metallization potential barrier, appearing dark due to increased current injection at this spot.

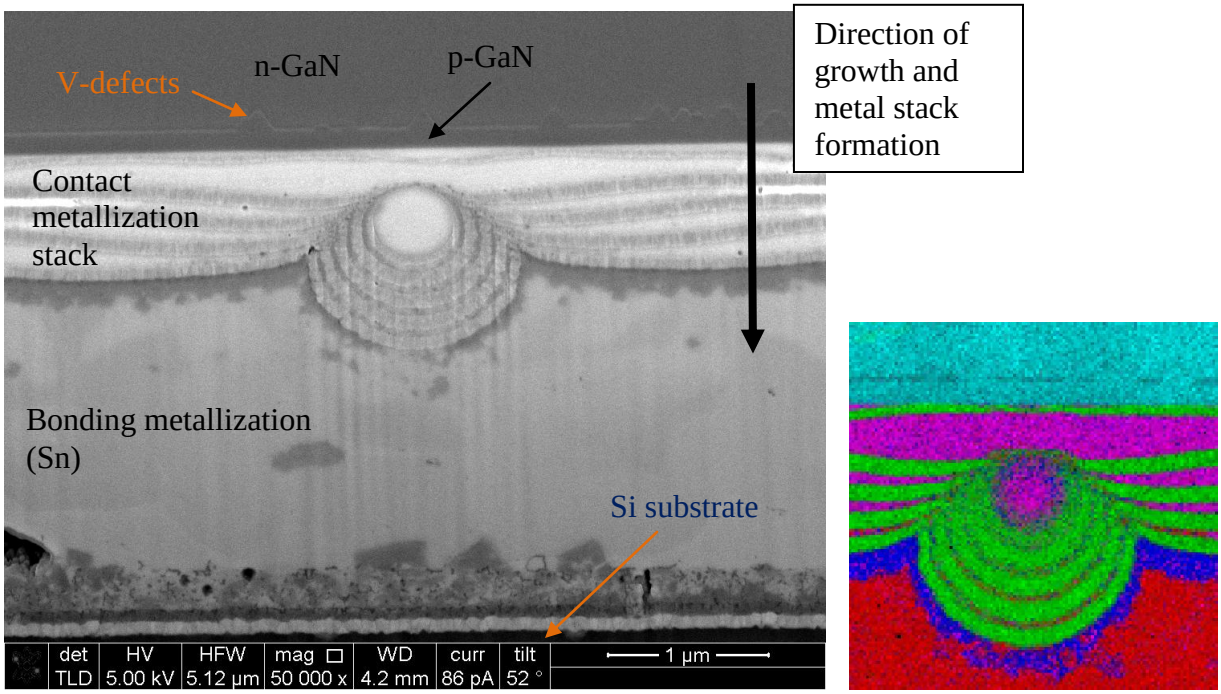

Figure 18. The left image is a cross-sectional SEM image of a stressed green LED showing a contact metallization defect. The right image shows TEM cross-sectional EDS mapping of different elements in the structure (Red = Sn, Blue = Pt-Sn-Ti, Green = W (Ti), Magenta = Pt-Sn, and Cyan = GaN)

When comparing the AVMs of these large dark defect spots to those AVMs of the same parts taken at time zero, it was determined that the bright defect spots observed at time zero were not

the origination of these defects. At the time intervals used to characterize the devices, no defect signal presented itself in that location until the macroscopic signal appeared in both the reflected light image and the AVM. The metallization defect itself (metal droplet with encompassing layers of metal) is likely present at time zero, given its geometry. Therefore this is a stress-activated defect. In a LE image of the green LED with this type of defect, this area appears dark likely due to the change in reflectivity of the metallization. Although some changes are seen in the optical image as well as the LE image, it took the TIVA/LIVA measurement to isolate the center of the defect. These high current density defects are present at time zero and activated under stress. They may cause premature failure in the green LEDs and/or reduction in efficiencies due to loss of reflectivity or change in spatial current distribution across the LED.

It was also of interest to determine the cause of the bright defect spot (with the halo) and the smaller dark defect spots that appeared upon aging of the device. The next figure, Figure 19, shows an AVM with two such defect signals. FIB cross-sectioning and TEM characterization were carried out on all three sites shown in the image. The following TEM images shown are all in an annular dark field (ADF) configuration which brings out the z-contrast in the image. Figure 20 shows the cross-section of the dark defect spot (labeled site 1 in Figure 19) and Figure 21 shows a cross-section of a bright defect spot with a halo. Note that site 2 is located within the haze and site 3 is not. There were not a lot of differences between the three sites. It was expected that site 1 would have a very different defect structure than those in sites 2 and 3 due to the dark versus bright contrast. This may have been the case and over etching of the TEM sample during FIB cross-sectioning through the defect signal may have removed the physical defect from the field of view in the TEM images. This is easy to do when the defect is very small. The dark spot in site 1 suggests a low resistance path through the device. In Figure 20 we do see a significant dislocation that penetrates from the removed substrate all the way into the p-GaN material. It is possible that metal extrusion from stress on the device enabled a shortage path down this dislocation causing an increased current path. However, no presence of metal was found along this dislocation with electron dispersive spectroscopy (EDS). If the dislocation alone caused significant band bending, it is possible that the 532 nm laser was enough to cause significant e-h pair generation at this site, compared to the slightly larger bandgap of the surrounding material. So even without metal in the core of the dislocation, band bending may be enough to cause a dark defect signal in the AVM. Still there were several other large dislocation cores observed in the TEM images that did not correlate to the presence of a dark dislocation spot in the AVM. Another theory for the presence of a dark defect signal would be the presence of a cluster of dislocations that caused more significant band bending than one core alone and generated the dark defect signal.

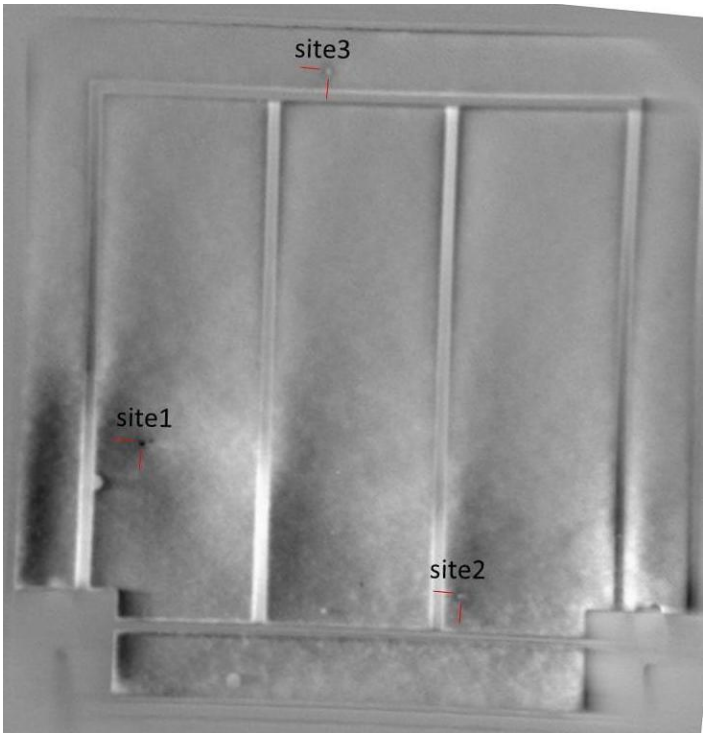

Figure 19. AVM of an aged green LED characterized by cross-sectional TEM at the three indicated sites

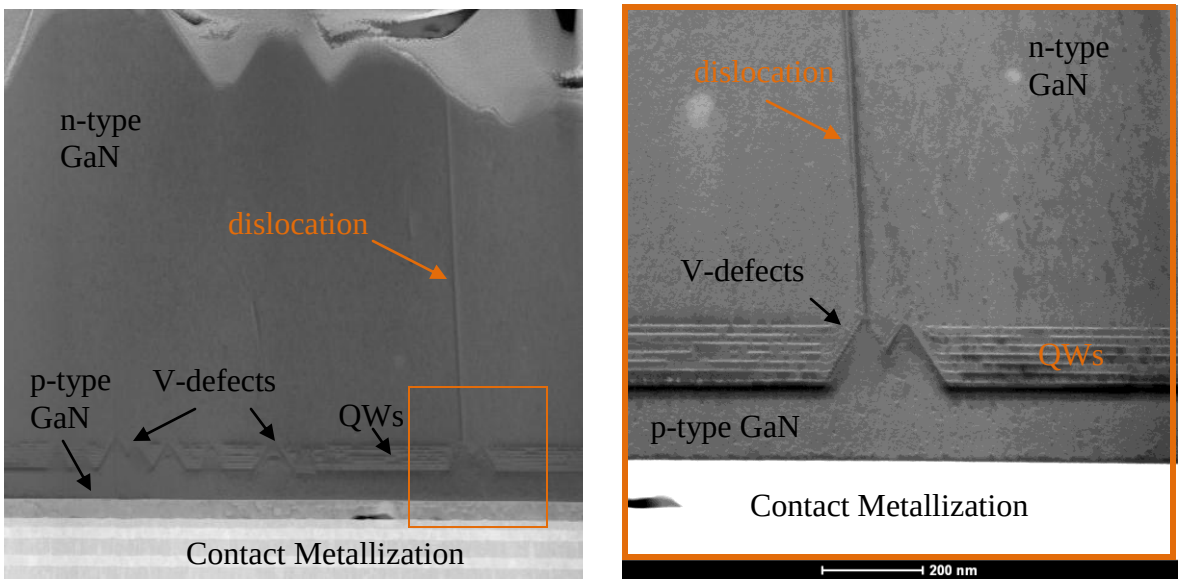

Figure 20. TEM images of the dark defect spot (site 1) indicated in Figure 19 (right image shows the orange box at a higher magnification)

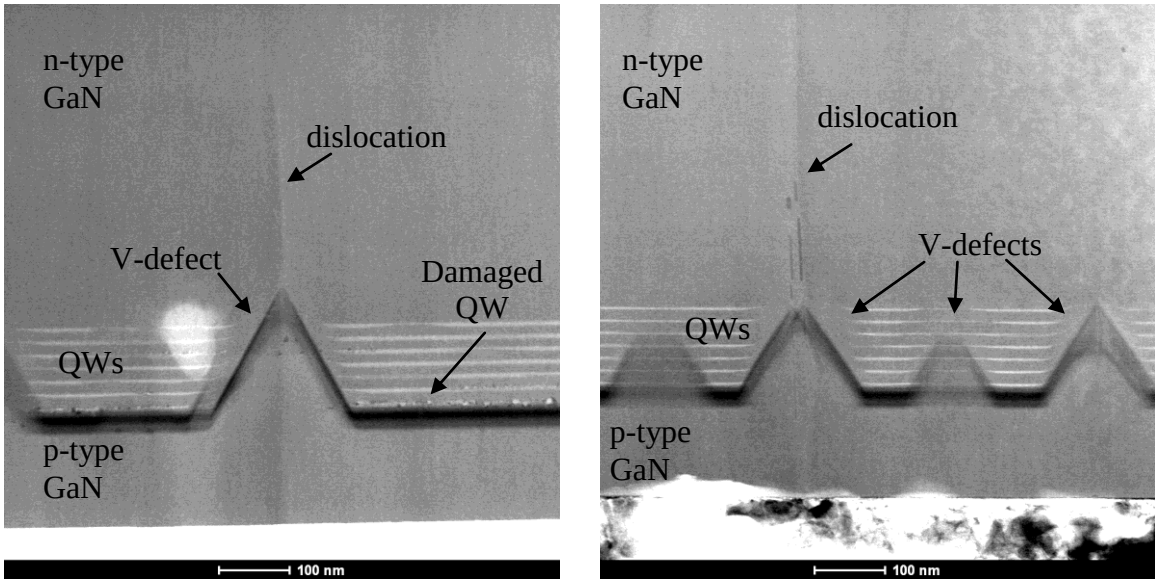

Figure 21. TEM cross-sectional images of site 2 (left) and site 3 (right) from Figure 19

In the case of site 2 and site 3, both show areas of threading dislocations through obvious V-defects in the quantum wells. The V-defects were ubiquitous throughout the cross-section, so the presence of the V-defects alone was not thought to cause the bright defect signal. Another interesting observation is the speckling behavior in the first QW shown in Figure 20 and in the left image of Figure 21 (sites 1 and 2). Both of these sites were defects that resided in the hazed region of the device. The speckling in the QW is not believed to be beam damage from FIB sample prep to the InGaN layers of the QW because all of the InGaN layers in the QWs would have been affected in a similar manner. This type of damage may be the cause of the hazed region of the chip. Unfortunately, the resolution of the TEM and subsequent beam damage at high magnifications made elemental determination of the speckled regions impossible. The speckling behavior was not observed at site 3 and this site was not removed from a haze region. As the first high In-content QW next to the p-type AlGaN, degradation of this layer may have a significant effect on the emission properties of the device.[14] This may account for the decreased emission in the LE images throughout the hazed region.

Over aging conditions that ranged from 150 mA to near to 350 mA without a heat sink, the TIVA/LIVA technique was able to successfully localize and monitor several types of defect signals. Due to the large sample size and critical attention to detail in the early stages of the aging process (multiple characterization steps at small time increments) and time constraints of outside organization materials characterization, it was difficult to fully characterize all of these defect types. However, from the characterization that was done, it is clear that any of these defects could potentially reduce efficiency and lifetimes of green LEDs. The TIVA/LIVA characterization technique provided a quick, efficient method of determining the number and type of defects at time zero and provided an easy method to monitor changes in these defects as the aging process progressed. However, it is still unclear the actual correlation between number and type of defects localized in the devices and early onset of failure in packaged devices. A next logical step in developing reliability FA capabilities for visible wavelength LEDs would be

to increase the statistics of this study and follow through with a greater number of cross-sectional TEM samples.

4.2 Degradation of UV LEDs

4.2.1. Stress Conditions and Changes over time

Unlike the green LEDs which were purchased in chip form, the UV LEDs came prepackaged with a heat sink. Thus they could be aged at the normal operating conditions without fear of thermal runaway. Of the 15 devices that were purchased, 6 were aged at 30 mA, 4 at 50 mA, and 2 at 70 mA. One device was aged at slight reverse currents and the rest were held as control samples. In the initial characterization of the devices, each of the UV LEDs was found to have 0-4 dark defect signals in their 532 nm AVMs. Therefore, the distribution was such that each of the aging conditions looked at one device with primarily active area defects and at least one with only mesa edge defects. Thus it could be determined if the spatial position of the dark defects contributed to early failure of the devices.

The IV curves and AVMs were monitored at every aging step. The spectra and EL emission were done intermittently at some aging steps to increase throughput. In the first few hours of aging at any current conditions, there appeared to be no change in the AVM. The spectra total emission tended to drop with time, but no obvious change in the AVM signal was observed. After nearly 20 hours of aging at 30 mA, one of the devices began to show signs of degradation. Before aging of this device, no AVM signal appeared at the defect site under reverse bias conditions and up to about 0.4 to 0.6 µA of applied current. The electrical aspects of the defect acted in part like a diode with a turn-on voltage. After a certain amount of applied bias, the defect turned on as a conductive path through the device. Now after aging, at slight reverse bias conditions (-0.6 µA, ~ -4.5 V) a bright spot appeared. Under a reverse bias, a bright spot again indicates increased current density or decreased resistance compared to the material around the defect spot. So the defect was starting to behave more like a linear short or a very leaky diode. The fact that the longer-wavelength lasers could also affect the dark defect spot at forward bias conditions indicated a leakage path through the device. Figure 22 shows the defect spot in a 532 nm AVM at both positive (middle image) and negative bias (right image) conditions. There is also a second defect spot shown in the middle AVM image (black arrow) under a positive 100 µA applied bias that does not change polarity under reverse bias. This second defect could be of a slightly different type from a mesa-edge defect, or the defect may not be as extensively damaged as the mesa-edge defect. Some of the other devices had AVM defect signals which exhibited the same behavior as the mesa-edge defect (changed polarity at reverse bias) with aging; other devices that failed did not. This behavior was also not constrained to mesa edge defects alone.

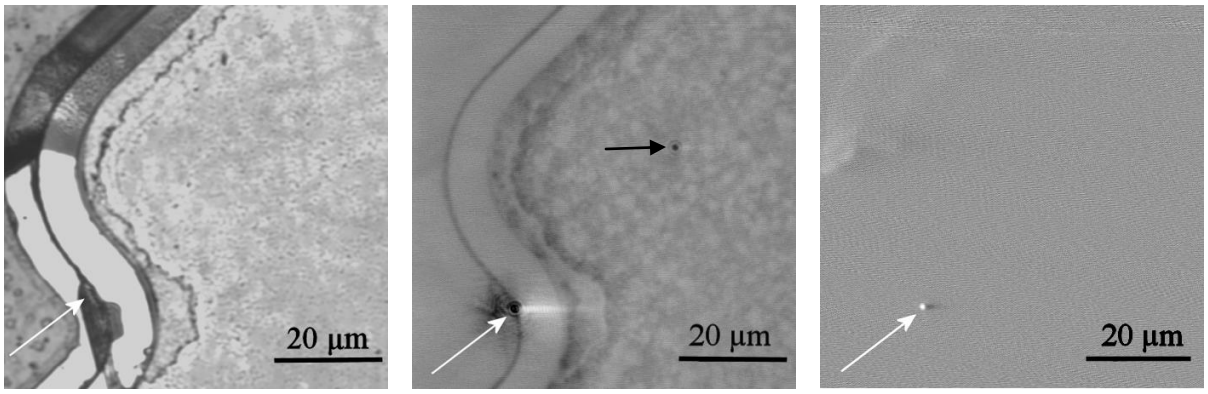

Figure 22. UV LED aged at 30 mA for 20 hrs showing the reflected light image (left), AVM at 100 µA (middle), and at -0.6 µA (right)

Other devices did not show changes in the initial dark defect spots but instead had new areas that became darker in contrast with aging time. In these cases, the new dark spots were not distinct like the dark defect spots obtained in the time zero AVMs. This larger dark area did not have the bias dependence that the distinct dark defect spots had, nor was it apparent under longer wavelength laser stimulation. These spots are likely due to p-type contact metal changes. They did not seem to directly relate to significant changes in the IV curves. An example of this is shown in Figure 23.

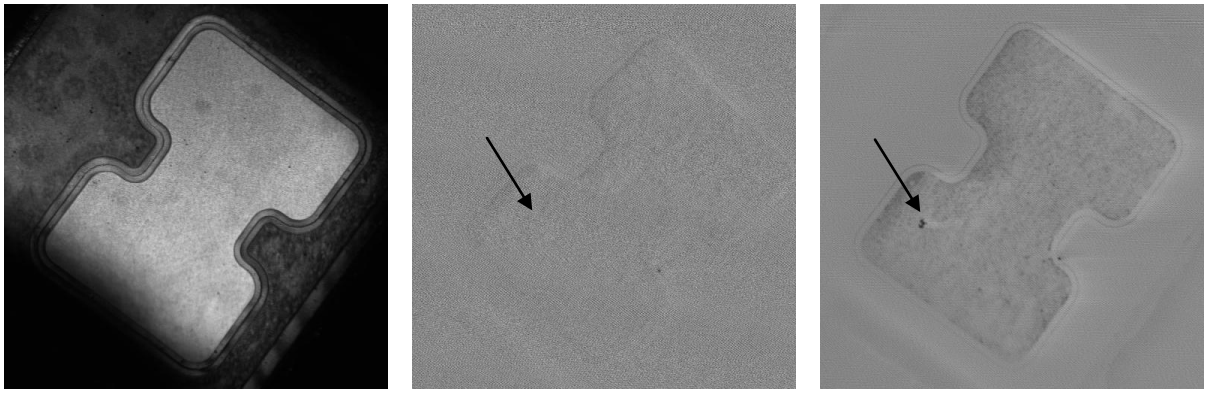

Figure 23. UV LED aged at 50 mA showing the differences between time zero (middle image) and after 2 hrs of aging (right image). The AVMs were taken with the 532 nm laser with 10 µA applied bias.

Another way that TIVA/LIVA was used to measure degradation of the UV LEDs was to monitor the relative increase in current that occurred by spotting the laser directly on the defect site. The current measured when the defect was stimulated with the 532 nm laser was compared to a control IV curve which was measured in the dark. Figure 24 shows the percent increase in current for one device measured after three aging times (0 hrs, 2 hrs, and 100 hrs at 30 mA). With laser stimulation, an increase in current is observed at reverse bias and up to about 3 V. The current increases with increased stress time. In this voltage range, stimulation from the laser affects the 'defect-free' area of the device in the same was as it does the defect (Figure 15, right image). One possibility is that an increase in leakage current could signify an increase in non-

radiative states that are created when electrons aggressively make it through the quantum wells and electron block into the p-type cladding layer.[10] What is unknown is in the voltage range of the secondary slope (3-4 V) why the increase in current at time zero is so much more than after aged conditions. This type of degradation monitoring by laser spotting is still in a preliminary stage and must be further developed. A potential outcome may be a screening process to determine a threshold increase in current at a defect site that above which a device will fail.

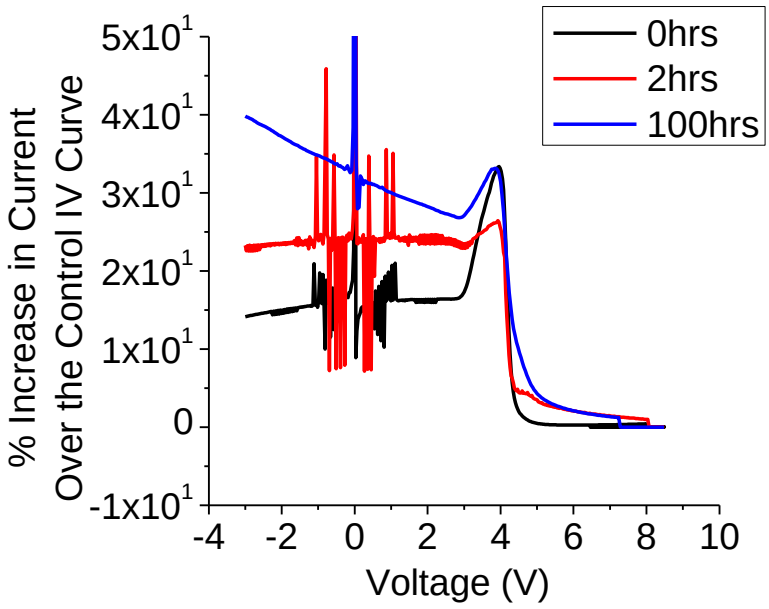

Figure 24. Percent current increase produced by the 532 nm laser spotted on the AVM dark defect signal above that of the control IV curve for three aging conditions

4.2.2. Failure in UV LEDs

Of the devices aged in this study (14), 6 failed within the first 150 hrs of aging at 30 mA, 50 mA, 70 mA or a slight reverse bias of -0.4 µA. The failure conditions are shown in Table 1. The number of TIVA/LIVA defect signals is also shown in the right three columns of

Table 1. The first column under the "Location of TIVA/LIVA Defect Signals" heading shows how many total defects were present in the device at time zero. The second and third columns define the location of those defects—whether they were in the active area of the structure or on the mesa edge. Only one of the parts stressed at 30 mA failed during aging. This occurred after 100 hrs. This particular chip had both an active area and a mesa edge defect. The only other part stressed at 30 mA with more active area defects was removed from the study prior to failure. Of those stressed at 50 mA, 3 out of 4 devices failed between 5 and 150 hrs. Of those devices, those with more defects failed (parts 1, 2 and 11), while the remaining device only had one defect present as a mesa-edge defect prior to stressing. Of the two devices stressed at 70 mA, only one failed after 15 hrs of stress. This failed device had more defects particularly in the active area than the one that did not fail. Only one part was stressed at slight reverse bias conditions, and it failed early on at 15 hrs. Given the limited statistics, the primary conclusion made is that more

initial defect spots observed in the AVMs led to earlier failures. Also that those parts with more active area defects (higher secondary slope and therefore increased leakage currents) tended to fail first. A greater sample set could increase confidence in this claim.

Table 1. Stress conditions of failed UV LEDs and the number of TIVA/LIVA defect signals at time zero

	Stress Condition at Room Temperature				Location of TIVA/LIVA Defect Signals		
Part#	30 mA	50 mA	70 mA	-0.4 μA	total #	# of active region	# of mesa edge
1		**Failed** at 5 hrs			2	1	1
2		**Failed** at 150 hrs			4	3	1
3	Removed from study at 5 hrs for TEM				4	2	2
4	200 hrs				2	1	1
5	**Failed** at 100 hrs				2	1	1
6	100 hrs				1	0	1
7		200 hrs			1	0	1
8	Control device--did not stress				0	0	0
9			**Failed** at 15 hrs		4	2	2
10			300 hrs		2	0	2
11		**Failed** at 15 hrs			1	1	0
12	Chip fell off						
13	200 hrs				0	0	0
14	150 hrs				1	1	0
15				**Failed** at 25 hrs	1	0	1

Failure in the UV LEDs after aging was typically very abrupt. Other than slight changes as mentioned in Section 4.2.1, aging usually brought about catastrophic failure in the devices: lack of emission, shorting behavior in the IV curves and multiple defect spot generation in the AVMs.

A couple of examples are shown in Figure 25. The middle column of images in this figure shows the AVMs with no applied bias. The right column shows the same device biased at 100 µA. With no applied bias, there are several bright defect signals that appear in each of the failed devices. The part with the most failure sites is that part that was aged under reverse bias conditions and not necessarily the one with the most defect signals at time zero. However, since only one part was aged in this fashion it is unreasonable to claim that there is a strong cause/effect relationship.

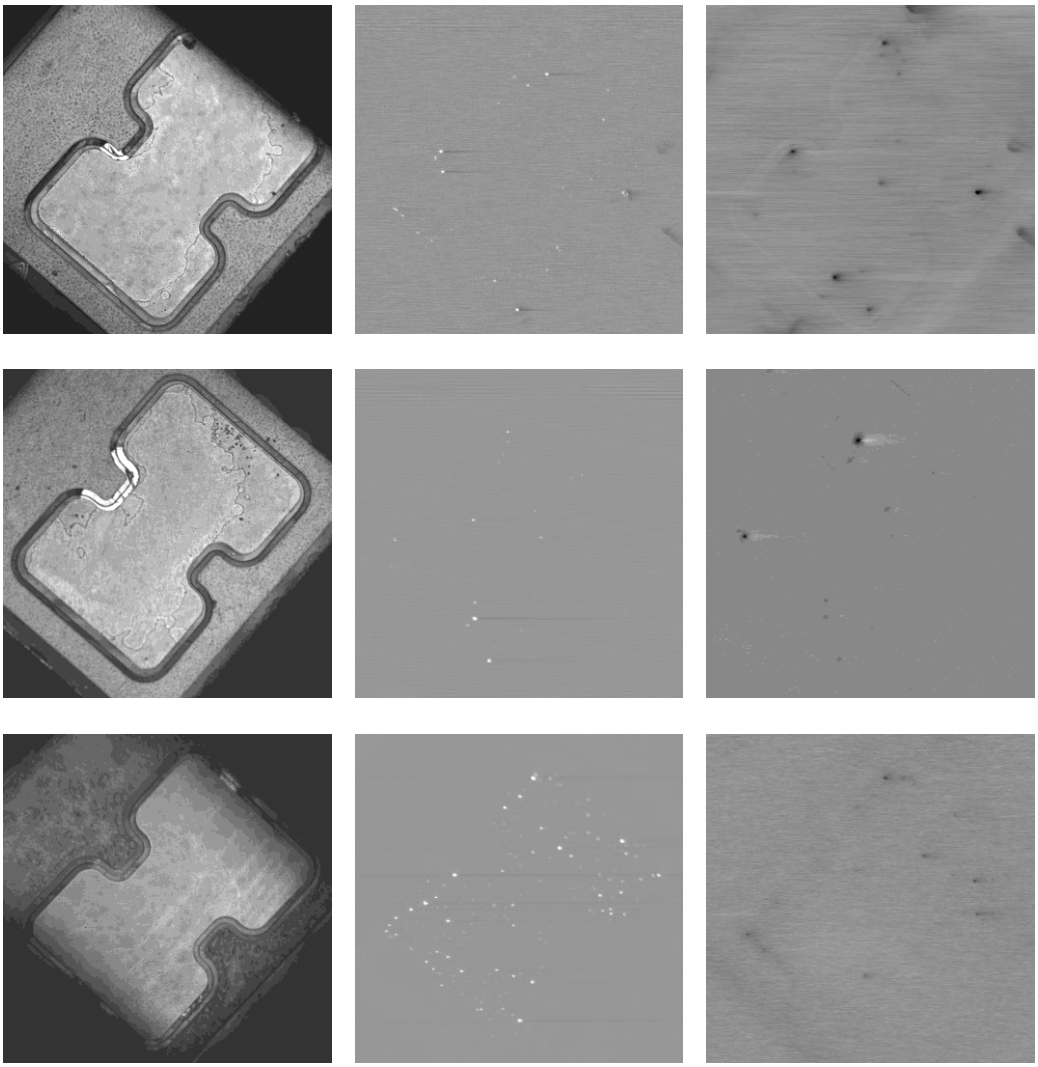

Figure 25. Reflected light images and corresponding 532 nm AVMs (middle column: 0 µA applied bias, right column: 100 µA applied bias) of three different stressed parts (top: 50 mA-2 hrs, middle: 30 mA-100 hrs, bottom: -0.4 µA-25 hrs)

Under increased bias conditions (third column in Figure 25 shows AVM at 100 µA) all of the bright defect spots change polarity and become dark defect spots. In other words as the bias is increased towards operating conditions all of the spots become leakage paths (low resistance paths). What is interesting is that some are much more intense than others suggesting that there

are defects that collect most of the charge flow, leaving other smaller defects with little leakage current and thus drowning out some of the original TIVA/LIVA dark defect signals.

The LE image of the top device in Figure 25 displayed an interesting behavior. Below about 1 mA of bias, no light emission spots were observed. At 1mA, several bright spots appeared matching many of the positions (but not all) of the dark spots in the top right image of Figure 25. Then at greater bias conditions (20 mA), the defect spots turned dark, as the emission from the rest of the device increased showing spatial degradation of the emitted light.

Still other parts which underwent catastrophic failure were found to only have a few defect signals with TIVA/LIVA signals as shown in Figure 26. In this case it is unlikely that characterization of the failure spot will give you more than evidence of what is left of a very high current density crater, not evidence of what might have led up to such an event. In this case characterization of the failure spot will most likely show severe damage at the failure site resulting from a high current short in the area. In addition, there are very few other defect spots visible, most likely because such a large defect contains all the charge flow and restricts that flow through other smaller defects. Notice also that the defect is clearly visible in the reflected light image. Two of the 15 parts had this type of behavior, the one shown in Figure 26 (50 mA for 15 hrs) and another part aged at 70 mA for 15 hrs.

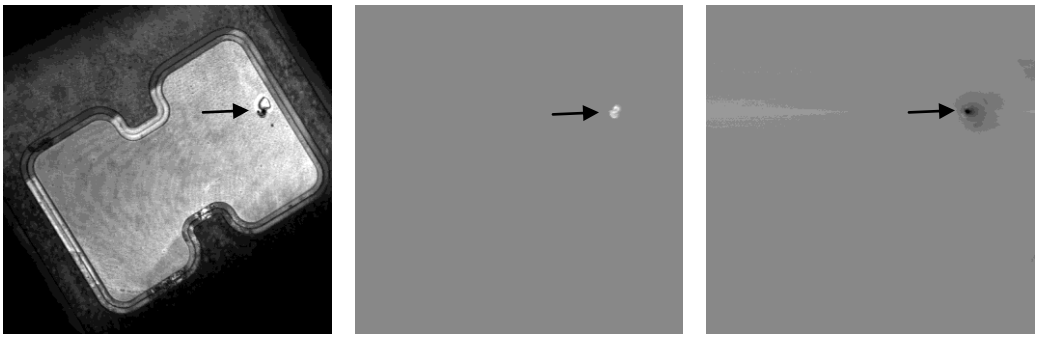

Figure 26. Aged UV LED at 50 mA for 15 hrs showing the one catastrophic failure site in both the reflected light image (left) and the AVMs (middle: no applied bias and right: 100 µA applied bias) with the 532 nm laser

4.2.3. Characterization of failed UV LEDs

Characterization of the UV LEDs with TEM proved a bit more difficult due to the thickness of the chip (~ 100 µm). They were flip-chipped, so what made the analysis of the devices with the SLM relatively easy made FIB extraction very difficult. The parts first had to be polished down to ~ 30µm of material. The devices then had to have power and ground connections rewired so that TIVA/LIVA could be performed to localize the defects. The FIB was then used to cut a hole in the material about 100 µm in width and length to take off another 20 µm of material before TEM sample preparation of the device. All of the sample preparation steps were necessary since the area of interest was most likely within the QWs or near the metal/semiconductor interface. Defects located only within the AlN or sapphire substrate and did not penetrate the *pn* junction of the diode might increase non-radiative defects, but would not have a great impact on the

electrical behavior of the device and therefore would not be present as electrically active defect signals in TIVA/LIVA.

Two UV LEDs were cross-sectioned and prepared for TEM imaging. The first was only aged minimally at 30 mA for 5 hrs. At the time, no drastic change had taken place in the AVM; only a slight drop in EL spectra intensity and minimal changes in the IV curves were observed. FIB cross-sectioning for TEM sample preparation focused on one of the dark defect signals observed in the AVM. The subsequent TEM image (Figure 27) showed that there was a very obvious dislocation in the area of interest, which terminated in something akin to a V-defect in InGaN material. The dislocation originated in the material below the superlattice, continued through the n-type AlGaN and terminated as a micropit located within the QW region. This image is rotated so the extent of the dislocation is clearly seen. The contact metallization is therefore on the left side of the image. At higher magnifications (normal orientation, second image in Figure 27), the QWs can be seen to turn and follow the V-shaped contour of the pit.

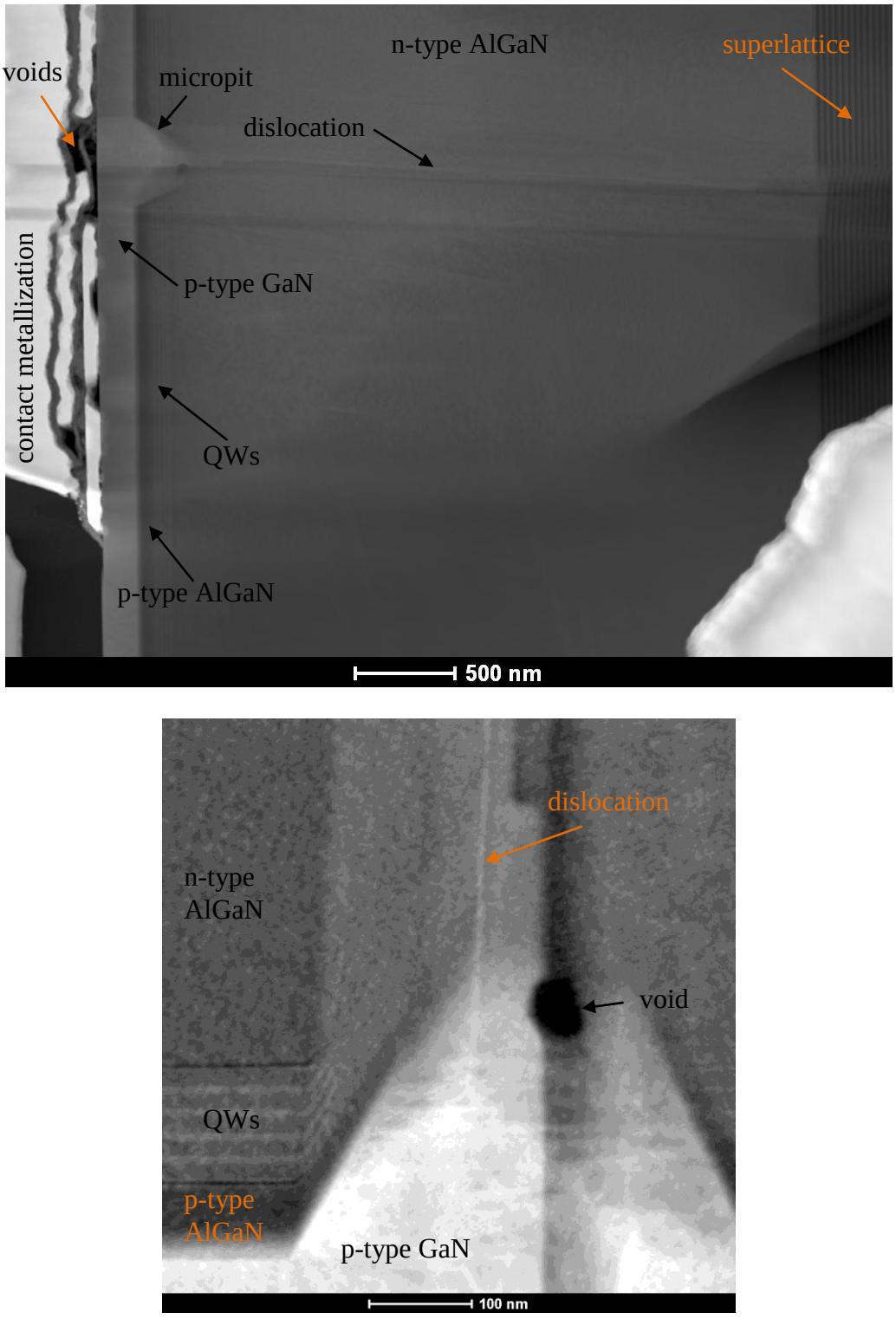

Figure 27. Top: TEM Cross-sectional image of an UV LED aged at 30 mA for 5 hours cut through a dark defect signal in the AVM (the image is rotated so that the growth direction is from the right to the left of the image); Bottom: TEM cross-sectional image showing a high magnification view of the defect (normal orientation)

As for the cause of the dark defect signal in the AVM for the UV LED, it is unlikely that band bending at the dislocation caused the dark defect signal. The bandgap energies of the AlGaN alloy layers in this device are much larger than the energy supplied by the 532 nm laser. Also, if band bending alone caused the signal, multiple dark defect signals would have shown up in the AVM. The reflected light image at high magnifications (Figure 12) indicated multiple optically-similar defects to the ones that gave off the electrically active signal. Electron dispersive spectroscopy (EDS) was performed within the micropit and along the dislocation core that extended through the n-type AlGaN from the disrupted superlattice. EDS indicated Ga enrichment and a trace of Au within the dislocation core. From the TEM image it is theorized that Au from the contact metallization diffused along the core to be found deep within the semiconductor structure. Metal that penetrates the QWs of the UV LED can be a shorting path along which leakage currents can pass. Within the contact metallization, the bright contrast layer was indeed Au and therefore the source of the metal within the dislocation core. In addition, voids within the Au layers as shown in the second image in Figure 27, are more evidence that the Au may have diffused down into the dislocation core from the contact metallization.

The second UV LED that was cross-sectioned for TEM analysis was the device depicted in the top row of Figure 25. This device was aged to failure at 50 mA for two hours. Again, the FIB was used to create a TEM sample of one of the dark defect spots (dark contrast at high currents). The TEM image is shown in Figure 28. This time, significant stress-induced dislocations and cracking was observed in the n-type AlGaN. This degraded area was centered on a bright contrast material which was identified as Au. There is no obvious dislocation core in this TEM image; the exact position of the dislocation was probably cut through during FIB etching for TEM sample preparation. From Figure 27 and from the presence of Au within the n-type AlGaN layer it is suggested that Au from the contact metallization diffused along a large dislocation core to cause the degradation deep within the n-type AlGaN. Voiding was observed in the contact metallization (Au layer) and what remains of a micropit within the p-type GaN layer. Failure conditions likely occurred when enough current could be injected through numerous dislocation cores along metal leakage paths to completely short the device. Metal extrusion down dislocation cores could explain the diode-like behavior of the dark defect signal. The metal/semiconductor potential barrier existed as a block to charge flow until the energy of the 532 nm laser combined with applied bias was enough to create a leakage path (turn-on voltage of ~3 V).

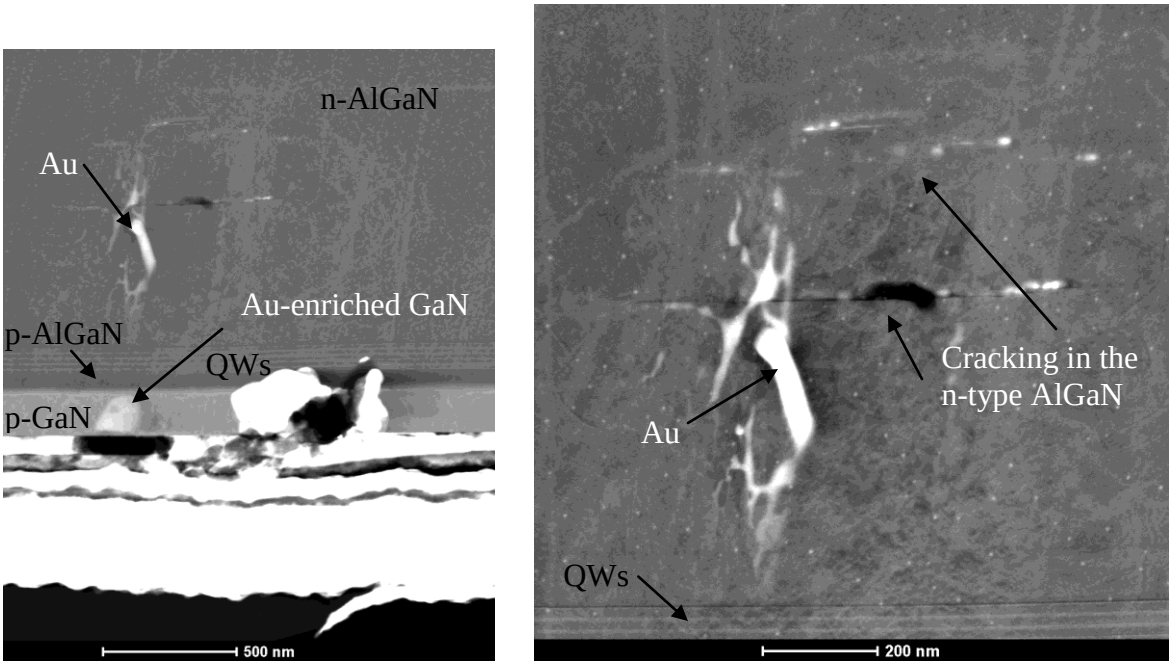

Figure 28. Cross-sectional TEM images of a failed UV LED aged at 50 mA for 5 hrs

Post failure, there were numerous defect signals detected in the AVM of the UV LEDs. Sometimes, the initial defect signal observed at time zero was not present in the post-failure AVM. The two TEM samples shown in the above figures suggest the same mechanism—a large micropit and dislocation are present allowing Au diffusion down the core. In the second image (Figure 28) there is extensive diffusion and damage. The strength of the AVM signal probably depended on the extent of Au diffusion down the cores. It is believed that all of the dark defect signals observed at time zero in the UV LEDs had a similar type of defect. Thus the TIVA/LIVA technique was able to determine those defects which were electrically active but not those defects which had the potential to become electrically active during accelerated stress conditions.

5. SUMMARY, CONCLUSIONS, AND FUTURE WORK

Through this early career LDRD project we have demonstrated that laser-based techniques (e.g. LIVA and TIVA) used in defect localization of silicon-based integrated circuits are effective in characterizing III-nitride LEDs. The focus in this work was on deep UV and deep green LEDs, which encompassed InGaN and AlGaN alloys. Regardless of the wavelength of the device, electrically active defect sites were localized in both deep UV and deep green LEDs. Once the defect sites were localized they were characterized with TEM cross-sections through the defective areas.

An approach to characterize the III-nitride LED devices with the laser-based FA techniques was developed. We systematically characterized both green and UV LEDs as a function of laser wavelength, biasing conditions and effect of laser stimulation on electrical measurements of the devices.

We developed a screening method that allows detection of electrically active defects in UV LEDs based on electrical characterization. The method can be easily performed without lengthy aging studies. Data from the electrical characterization could be used to predict the existence of defects in the UV LEDs.

In this preliminary work defects were observed in both the green and UV LEDs that could potentially reduce the lifetimes of the devices. In the green LEDs, dark defect signals observed using the laser-based localization techniques were used to pinpoint large contact metallization defects. Defects in the contact metallization and at the metal/p-type semiconductor interface may create strong spatial non-uniformities in current injection. This type of defect could create hotspots and non-uniform light emission. Dark defect signals observed in the UV LEDs were determined to be shorting paths. Part of the contact metallization had diffused along dislocation cores to create leakage currents through the quantum wells. It is theorized that failure occurred in the UV LEDs when enough of these leakage paths dominated current injection through the QWs.

Further pursuit of this work may take one of several directions. This preliminary work was able to isolate defect signals at time zero and monitor changes over stress time. However due to the number of samples characterized and limited materials characterization, a few questions were left unanswered. The cause of the bright defect spots in the green LEDs at time zero is still unclear; increased materials characterization may reveal additional information. The cause of the small dark defect spots (low resistance paths) also remains uncertain. TEM cross-sections revealed dislocation cores and V-defects, but nothing structurally significant to separate the dark defect spots from the bright ones. Point defects may be the culprits. Packaged green LED devices may also be desirable for further work to reduce effects of thermal degradation on the devices. For the UV LEDs, it is clear that a dislocation is present at the failure site and that Au has diffused through the QW. However, it is still unclear what materials property the dislocation possessed to segregate itself from surrounding dislocations (size, presence of a micropit). Plan-view TEM may reveal another dimension of structure that is required for this type of failure to take place. One theory might be a cluster of dislocations. Finally the laser-spotting technique shows merit in monitoring degradation of the UV LEDs by observing change in leakage current

stimulated by the laser. A quantitative correlation between increases in leakage current under laser stimulation and time to failure would be beneficial to monitor degradation of the devices.

In this work we have proven that the TIVA/LIVA characterization technique can be a successful tool for III-nitride LED characterization of defects and degradation. Other devices that may benefit from this characterization technique are III-nitride laser diodes and high electron mobility transistors. It is also possible that this technique could be applied to other III-V devices with indirect bandgaps such as SiC, encouraging collaborations with power electronics development as well as optoelectronics. Coupled with other electrical measurements, the TIVA/LIVA technique can be a powerful tool to predict early failure in commercial devices as well as support the development of in-house semiconductor devices. Further studies characterizing the multiple different defects observed in the green and UV LEDs and further laser-spotting characterization are expected to fully establish the TIVA/LIVA technique as a viable screening method and reliability technique for III-nitride optoelectronics.

6. REFERENCES

1. A. Khan, S. Hwang, J. Lowder, V. Adivarahan, and Q. Fareed, Proc. Int. Rel. Phys. Symp. **47**, 89 (2009).
2. M. Meneghini, A. Tazzoli, G. Mura, G. Meneghesso, and E. Zanoni, IEEE Trans. Electron Dev. **57**, 108 (2010).
3. A. Pinos, S. Marcinkevičius, J. Yang, Y. Bilendo, M. Shatalov, R. Gaska, and M.S. Shur, Appl. Phys. Lett. **95**, 181914 (2009).
4. S. Sawyer, S.L. Rumyantsev, and M.S. Shur, Solid-State Electron. **52**, 968 (2008).
5. C.G. Moe, M.L. Reed, G.A. Garrett, A.V. Sampath, T. Alexander, H. Shen, M. Wraback, Y. Bilenko, M. Shatalov, J. Yang, W. Sun, J. Deng and R. Gaska, Appl. Phys. Lett. **96**, 213512 (2010).
6. X.Z. Cao, P.M. Sandvik, S.F. LeBoeuf, S.D. Arthur, Microelectron. Reliab. **43,** 1987 (2003).
7. A. Chitnis, J. Sun, A. Mandavilli, R. Pachipulusu, S. Wu, M. Gaevski, v. Adivarahan, P.P. Zhang, M.A. Khan, A. Sarua, and M. Kuball, Appl. Phys. Lett. **81**, 3491 (2002).
8. M.L. Reed, M. Wraback, A. Lunev, Y. Bilenko, X. Hu, A. Sattu, J. Deng, M. Shatalov, and R. Gaska, Phys. Status Solidi C **5**, 2053 (2008).
9. A. Pinos, S. Marcinkevičius, and M.X. Shur, J. Appl. Phys. **109**, 103108 (2011).
10. A. Pinos, S. Marcinkevičius, J. Yang, R. Gaska, M. Shatalov, and M.X. Shur, J. Appl. Phys. **108**, 093113 (2010).
11. D.K. McElfresh, and D. Vacar, Appl. Phys. Lett. **86**, 22108-1-3 (2005).
12. R.W. Herrick, Microelectronics Failure Analysis, 5th Edition, ASM International (2004), 229-252.
13. D.L. Barton, M. Osinski, C.J. Helms, N.H. Berg, and B.S. Phillips, Proc. SPIE **2693**, 64 (1995).
14. A. David, M.J. Grundmann, J.F. Kaeding, N.F. Gardner, T.G. Mihopoulos, and M.R. Krames, Appl. Phys. Lett. **92**, 053502 (2008).

DISTRIBUTION

1	MS1071	Clinton A. Boye	01720 (electronic copy)
1	MS1072	Edward I. Cole, Jr.	01726 (electronic copy)
1	MS1081	Guillermo M. Loubriel	01726 (electronic copy)
1	MS1081	Paiboon Tangyunyong	01726 (electronic copy)
1	MS1086	Mary A. Miller	01726 (electronic copy)
1	MS0359	D. Chavez, LDRD Office	01911
1	MS0899	RIM-Reports Management	9532 (electronic copy)


Sandia National Laboratories